S1 Supplemental information to Section 1 - Introduction

Table S1 Overview (non-exhaustive) of earlier studies based on TM5-FASST

	Scope	$PM_{2.5}$ and O_3 exposure detail	Climate metrics	Health impact	Crop impact
Kuylenstierna et al., 2011; The World Bank, The International Cryosphere Climate Initiative, 2013	Near-Term Climate protection and Clean Air Benefits: Actions for Controlling Short-Lived Climate Forcers	5 world regions	yes*	External assessment, TM5-FASST used for attribution by measure, by region based on PM2.5	yes
Brauer et al., 2012; Cohen et al., 2017; Lim et al., 2012	Air pollution exposure assessment for Global Burden of Disease	Grid maps	no	External assessment based on TM5-FASST $PM_{2.5}$ and O_3 grid maps	no
Rao et al., 2016	A multi-model assessment of the co-benefits of climate mitigation for global air quality	Grid maps and World regions	no	Population exposure to $PM_{2.5}$ limit levels	no
Crippa et al., 2016	Retrospective analysis of European air quality policies versus hypothetical non-action	World regions	no	Change in statistical life expectancy	yes
OECD, 2016	The Economic Consequences of Air Pollution	Grid maps and World regions	no	External assessment based on TM5-FASST $PM_{2.5}$ and O_3 grid maps	yes
UNEP and CCAC, 2016	Integrated Assessment of Short-Lived Climate Pollutants for Latin America and the Caribbean	Grid maps	yes*	yes	yes
van Zelm et al., 2016	Regionalized characterisation factors for Life Cycle Analysis based on TM5-FASST source-receptors	FASST regions	no	yes	yes
Rao et al., 2017	Future air pollution in the Shared Socio-economic Pathways	Grid maps and World regions	no	Population exposure to $PM_{2.5}$ limit levels	No
Kitous et al., 2017	Global Energy and Climate Outlook 2017: How climate policies improve air quality	Grid maps and World regions	no	External based on TM5-FASST $PM_{2.5}$ and O_3 grid maps	yes

* In the 2 assessments where climate metrics were evaluated, the BC forcing was adjusted with a correction factor 3.6 relative to the default FASST BC forcing (see main text)

S2 Supplemental information to section 2.1 –The native TM5 model

S2.1 Features of the native TM5 model

TM5-CTM is an off-line global transport and chemistry model (Huijnen et al., 2010; Krol et al., 2005) that mainly uses the ECMWF operational or re-analysed meteorological data. In this study the operational 12-hour IFS forecast product for the year 2001 has been utilized. We used the year 2000 of the 0.5x0.5 degree historical gridded anthropogenic emission data described by Lamarque et al. (2010) as the basis for our calculations. Components used were NO_x, NMVOC, NH_3, SO_2, OC, and BC, and gridding was done using RETRO and EDGAR-HYDE database. The choice for this reference emission dataset was motivated by the fact that this dataset was widely used as the 'handshake' between past- and future emission inventories in the activities informing the IPCC AR5 process.

Large scale biomass burning emissions of BC and POM are from (van der Werf et al., 2004); Organic aerosols are assumed to be emitted as primary following Dentener et al., (2006); dust and sea salt emission schemes are also from Dentener et al., (2006).

Model calculations were performed for 1 calendar year, with a spin-up of 6 months for the base-simulations, and 1 month for the perturbation simulations, justified by the fact that the perturbations were performed for components with lifetimes of hours to a few days (no simulations for CO and CH4). TM5-CTM has a spatial global resolution of 6°×4° and a two-way zooming algorithm that allows regions (e.g. Europe, N. America, Africa, and Asia) to be resolved at a finer resolution of 1°×1°. To smooth the transition between the global 6°×4° region and the regional 1°×1° domain, a domain with a 3°×2° resolution has been added. The TM5 version used here has a vertical resolution of 25 layers, defined in a hybrid sigma-pressure coordinate system with a higher resolution in the boundary layer and around the tropopause. The height of the first layer is approximately 50 m.

TM5-CTM uses the first-moments "slopes" scheme for the advection calculations (Petersen et al., 1998; Russell and Lerner, 1981). The model transport has been extensively validated using ^{222}Rn and SF6 (Peters, 2004) and further validation was performed within the EVERGREEN Project (Bergamaschi et al., 2005).

Gas phase chemistry is calculated using the CBM-IV chemical mechanism (Gery et al., 1989a, 1989b) modified by Houweling et al. (1998), solved by means of the EBI method (Hertel et al., 1993). Dry deposition is calculated using the ECMWF surface characteristics and Wesely's resistance method (Ganzeveld and Lelieveld, 1995)

The inorganic aerosol compounds, sulphate (SO_4^{2-}), nitrate (NO_3^-) and ammonium (NH_4^+), are assumed internally mixed and in thermodynamical equilibrium, while black carbon (BC), particulate organic matter (POM), sea salt and dust are externally mixed. Sulphate, nitrate, ammonium, BC and POM are considered to be in the accumulation mode components and are considered only by mass. Sea salt and dust are described by two log-normal distributions, using two modes for each of the species: accumulation and coarse modes.

Wet deposition is the dominant removal process for most aerosols and therefore is a major source of uncertainty in aerosol modelling (Textor et al., 2006). Removal occurs in convective systems (convective precipitation) and in large-scale

stratiform systems that are associated with weather fronts. The in-cloud removal rates, which depend on the precipitation rate are differentiated for convective and stratiform precipitation and are calculated following Guelle et al. (1998) and Jeuken et al. (2001). Aerosol below-cloud scavenging is parameterised according to Dana and Hales (1976).

The model results have been evaluated in model inter-comparison exercises (Textor et al., 2006), using in-situ, satellite and sun-photometer measurements (De Meij et al., 2006; Vignati et al., 2010), summarized in Table S2.1 below.

Table S2.1: Overview of validation studies of the chemistry-transport model TM5

Reference	Validation type	Major outcome
Van Dingenen et al. (2009)	TM5 regionally averaged monthly O_3 and O_3 metrics against observations (year 2000)	TM5 monthly O_3 and crop metrics generally within variability of observations in US, SE-Asia and Europe (except over-estimated AOT40 in Central Europe), underestimating monthly O3 observations in India and Africa.
De Meij et al. (2006)	Comparison of AOD with AEROCOM and MODIS over Europe.	Underestimated of AERONET AOD values by 20–30%, high spatial correlation with MODIS. Column aerosol small dependency on emission inventory.
van Noije et al., 2006	Comparison of ensemble of models to multiple NO_2 satellite derived columns.	High spatial correlation of all models (including TM5) with satellite observations- large difference in retrievals precluded identification of systematic differences. Underestimate of NOx retrieval in China and South Africa.
Dentener et al., 2006	Evaluation of ensemble of models over world regions.	In regions with observations, TM5 was one of the best performing models due to relatively high resolution. In other regions, larger deviations- in line with other models.
Shindell et al., 2008	Evaluation of CO, ozone, BC and Sulfate transport over the Arctic	Poor representation of reactive tracer transport by all models to 4 Arctic stations.
Brauer et al., 2016	$PM_{2.5}$ from worldwide-database of urban and rural stations.	Similar performance of TM5 with regard to satellite derived surface PM

Table S2.2 Definition of TM5- FASST master zoom areas, source regions and individual countries included

MASTER 1°x1° ZOOM WINDOW		FASST SOURCE REGIONS IN ZOOM	COUNTRIES IN FASST REGION	COUNTRIES ISO CODE
AFR	AFRICA	EAF	Eastern Africa	CAF TCD SDN ETH SOM KEN UGA COD RWA TZA MDG ERI DJI COM BDI BID MUS REU SYC SDS SOL
		NOA	Morocco, Tunisia, Libya and Algeria	MAR DZA ESH TUN LBY SAH
		SAF	Southern Africa (excl. RSA)	AGO NAM ZMB BWA ZWE MOZ MWI MYT
		WAF	West Africa	COG CNQ GAB GIN CMR NGA NER MLI BEN GHA BFA CIV SEN GMB GNB SLE LBR STP CPV SHN TGO GNQ MRT
AUS	AUSTRALIA	AUS	Australia	AUS
		NZL	New Zealand	NZL
EAS	EAST ASIA	CHN	China, Hong Kong and Macao	CHN HKG MAC
		COR	South Korea	KOR
		JPN	Japan	JPN
		MON	Mongolia and North Korea	MNG PRK
		TWN	Taiwan	TWN

(continues on next page)

Table S2.2 Cont'd

MASTER 1°x1° ZOOM WINDOW		FASST SOURCE REGIONS IN ZOOM	COUNTRIES IN FASST REGION	COUNTRIES ISO CODE
MASTER 1°x1° ZOOM WINDOW		FASST SOURCE REGIONS IN ZOOM	COUNTRIES IN FASST REGION	COUNTRIES ISO CODE
EUR	EUROPE	AUT	Austria, Slovenia and Liechtenstein	AUT SVN LIE
		BGR	Bulgaria	BGR
		BLX	Belgium, Luxemburg and Netherlands	BEL LUX NLD
		CHE	Switzerland	CHE
		ESP	Spain and Portugal	ESP PRT GIB
		FIN	Finland	FIN
		FRA	France and Andorra	FRA AND
		GBR	Great Britain and Ireland	GBR IRL GGY IMN JEY
		GRC	Greece and Cyprus	GRC CYP
		HUN	Hungary	HUN
		ITA	Italy, Malta, San Marino and Monaco	ITA VAT SMR MCO MLT
		NOR	Norway, Iceland and Svalbard	NOR ISL SJM
		POL	Poland and Baltic states	POL EST LVA LTU
		RCEU	Serbia, Montenegro, Macedonia and Albania (Rest of Central Europe)	SCG MKD HRV BIH ALB SRB MNE
		RCZ	Czech Republic and Slovakia	CZE SVK
		GER	Germany	DEU
		ROM	Romania	ROU
		SWE	Sweden and Denmark	SWE DNK FRO

(continues on next page)

Table S2.2 Cont'd

MASTER 1°x1° ZOOM WINDOW		FASST SOURCE REGIONS IN ZOOM	COUNTRIES IN FASST REGION	COUNTRIES ISO CODE
MAM	CENTRAL AMERICA	MEX	Mexico	MEX
		RCAM	Central America and Caribbean	PAN NIC HND GTM SLV ANT KNA LCA VCT TTO TCA VIR BLZ AIA ATG ABW BHS BRB VGB CYM DMA CUB DOM GRD GLP HTI JAM MTQ MSR PRI CRI
MEA	MIDDLE EAST	EGY	Egypt	EGY
		GLF	Gulf states	BHR IRQ KWT OMN QAT SAU ARE YEM IRN
		MEME	Israel, Jordan, Lebanon, Palestine Territories and Syria (Near East)	ISR JOR PSE LBN SYR PSX
		TUR	Turkey	TUR
NAM	NORTH AMERICA	CAN	Canada and Greenland	CAN GRL
		USA	United States	USA SPM BMU

Table S2.2 Cont'd

MASTER 1°x1° ZOOM WINDOW		FASST SOURCE REGIONS IN ZOOM	COUNTRIES IN FASST REGION	COUNTRIES ISO CODE
MASTER 1°x1° ZOOM WINDOW		FASST SOURCE REGIONS IN ZOOM	COUNTRIES IN FASST REGION	COUNTRIES ISO CODE
RSA	SOUTH AFRICA	RSA	Republic of South Africa, Swaziland and Lesotho	ZAF SWZ LSO
RUS	FORMER SOVIET UNION	KAZ	Kazachstan	KAZ
		RIS	Rest of former Soviet Union	KGZ TKM UZB TJK
		RUE	Eastern part of Russia	RUE
		RUS	Russia, Armenia, Georgia and Azerbeijan	RUS ARM GEO AZE
		UKR	Ukraine, Belarus and Moldovia	BLR MDA UKR
SAM	SOUTH AMERICA	ARG	Argentina, Falklands and Uruguay	ARG FLK URY
		BRA	Brazil	BRA
		CHL	Chile	CHL
		RSAM	Rest South America	BOL COL ECU GUF GUY PER SUR VEN PRY PRA
SAS	SOUTH ASIA	NDE	India, Maldives and Sri Lanka	IND LKA MDV
		RSAS	Rest of South Asia	AFG BGD BTN NPL PAK
SEA	SOUTHEAST ASIA	IDN	Indonesia and East Timor	IDN TLS
		MYS	Malaysia, Singapore and Brunei	MYS SGP BRN
		PHL	Philippines	PHL
		RSEA	Cambodia, Laos and Myanmar	KHM LAO MMR
		THA	Thailand	THA
		VNM	Vietnam	VNM
PAC	PACIFIC	PAC	Pacific Islands and Papua New Guinea	FJI NCL SLB VUT FSM GUM KIR MHL NRU MNP PLW NFK TKL ASM COK PYF NIU PCN TON TUV WLF WSM PNG

S3 Supplemental information to section 2.3 - Air pollutants source-receptor relations

Table S3 Overview of additional perturbation experiments for selected regions, in addition to the 20% perturbation for the standard source-receptor simulations

			Emission perturbation magnitude relative to base simulation			
Source region	Simulation code	Compounds perturbed	-80%	-50%	+50%	+100%
EUR MASTER ZOOM	P3	NO_x	X	X	X	X
REGION	P5	NO_x+NMVOC	X			X
	P4	NH_3+NMVOC	X			X
	P2	SO_2	X			X
GERMANY	P3	NO_x	X	X	X	X
	P5	NO_x+NMVOC				
	P4	NH_3+NMVOC	X			X
	P2	SO_2	X			X
USA	P3	NO_x	X	X	X	X
	P5	NO_x+NMVOC	X			X
	P4	NH_3+NMVOC				
	P2	SO_2	X			X
CHINA	P3	NO_x	X	X	X	X
	P5	NO_x+NMVOC	X			X
	P4	NH_3+NMVOC	X			X
	P2	SO_2	X			X
JAPAN	P3	NO_X	X	X	X	X
	P5	NO_x+NMVOC				
	P4	NH_3+NMVOC	X			X
	P2	SO_2	X			X
INDIA	P3	NO_X	X	X	X	X
	P5	NO_x+NMVOC	X			X
	P4	NH_3+NMVOC	X			X
	P2	SO_2	X			X

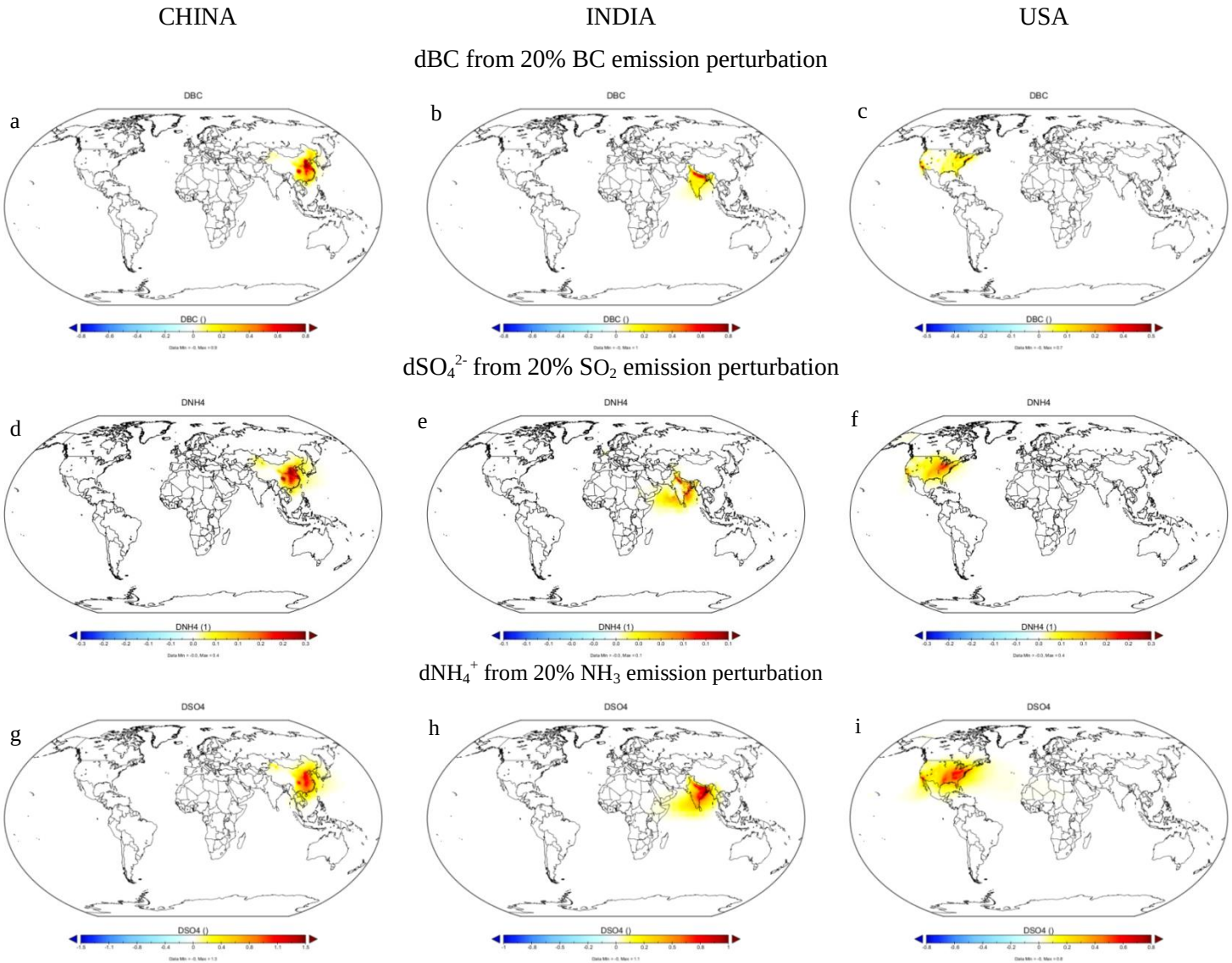

Figure S3.1 Change (reversed sign) in annual mean surface BC (a to c), SO_4^{-2} (d to f) and NH_4^+ (g to i) response for a 20% decrease in year 2000 emissions of selected precursors from source regions China, India and USA respectively

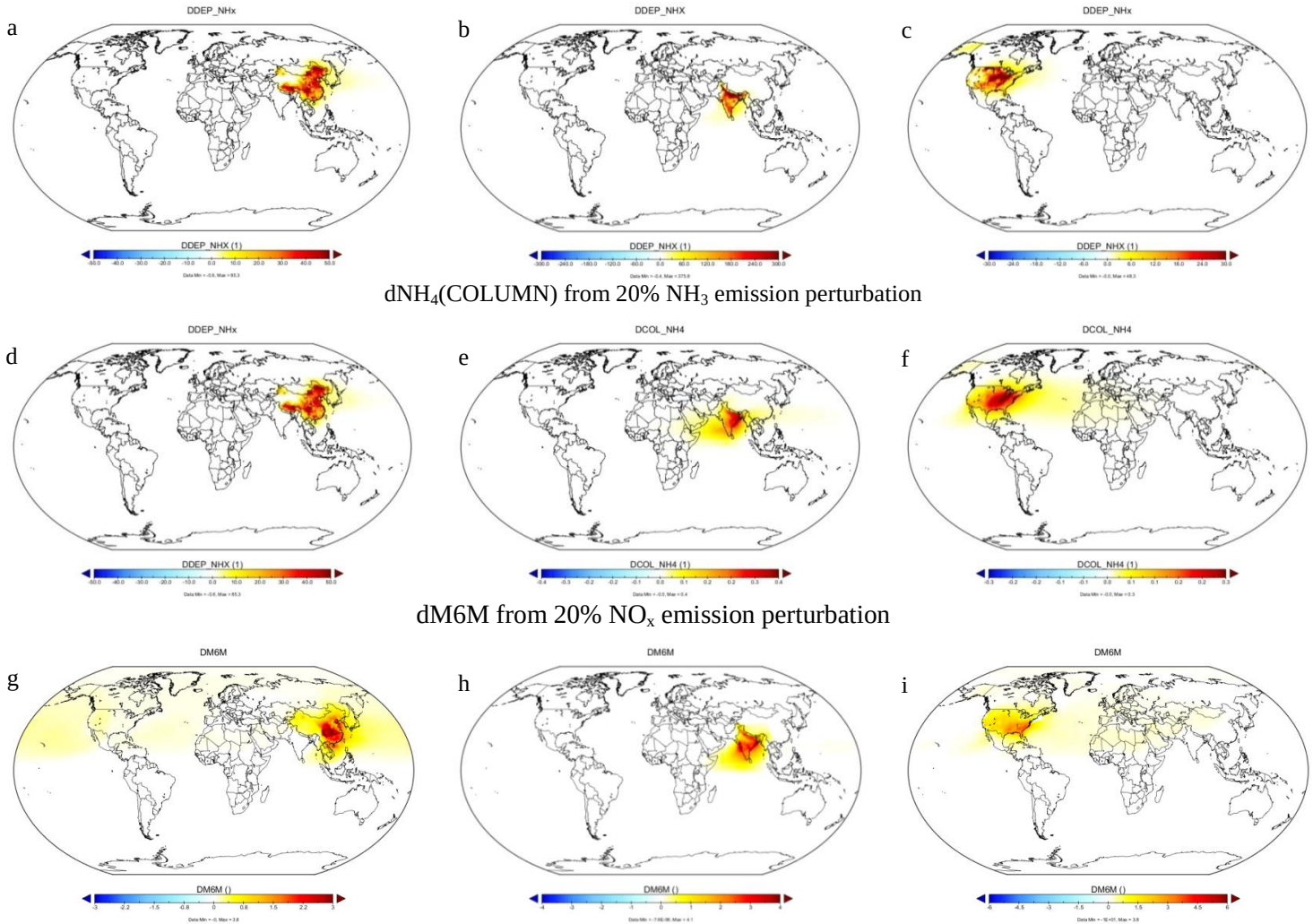

Figure S3.2 Change (reversed sign) in annual deposition (a to c) , total column burden (d to f) and ozone exposure metric M6M (g to i) response for a 20% decrease in year 2000 emissions of NH_3 (a to f) and NO_x (g to i) from source regions China, India and USA respectively

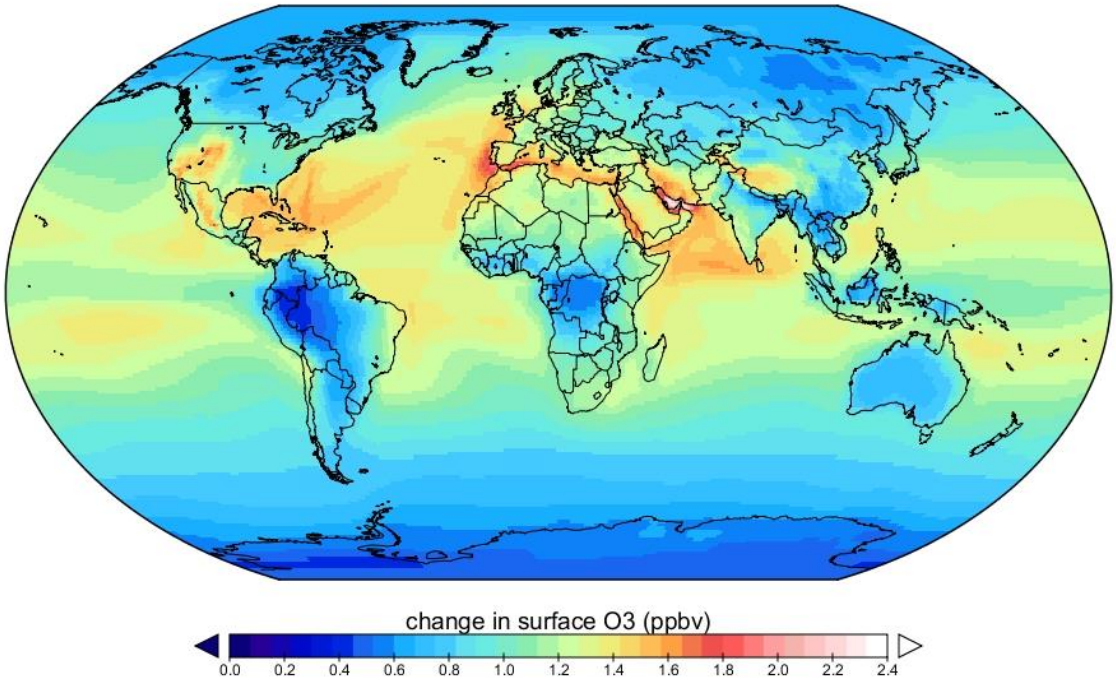

Figure S3.3 Change (reversed sign) in annual mean surface O_3 for a 20% decrease in year 2000 CH4 concentration, i.e. 1760 to 1408 ppb (TF-HTAP1 SR1-SR2 scenarios)

S4 Supplemental information to section 2.4 – Urban increment

S4.1 Methodology for the calculation of the urban increment adjustment factor for primary PM2.5

Previous studies have developed methodologies to calculate the so-called urban increment for some European cities (Amann et al., 2007), but at present no globally applicable simple method is available. Therefore, within TM5-FASST a parameterization was developed to adjust the gridcell area-averaged $PM_{2.5}$ concentration to a more appropriate population-averaged urban background concentration, accounting for the sub-grid gradient in population distribution and pollutant concentrations. The urban increment correction will be applied to primary $PM_{2.5}$ only, as secondary $PM_{2.5}$ species (sulphate and nitrate) are formed from chemical conversion mechanisms over larger time and spatial scales, i.e. secondary $PM_{2.5}$ species are expected to be more homogeneously mixed over the native gridcell. It has to be noted that exposure to O_3 in urban areas will rather be overestimated using the gridcell average, because of O_3 titration inside traffic-dominated areas. Sub-grid effects on O_3 and NO_x are currently not taken into account in our approach.

In brief, the method relies on high spatial resolution population statistics from which the urban area fraction and urban population fraction inside each native 1°x1° gridcell are calculated. TM5-FASST has the choice of 2 families of population datasets, listed in Table S5.1.

The CIESIN Global Population of the World (GWPv3) set has the advantage of very high resolution, but lacks projected data beyond 2015[1]. The GEA - UN dataset (provided via personal communication by S. Rao, 2009) has a more limited spatial resolution but contains projections until 2100 in decadal steps from 2010 onwards. Further, the GEA - UN dataset contains already information on the urban population fraction, whereas the CIESIN dataset provides only count and density, and needs further assumptions and processing to derive the urban population.

Defining the urban area and population fraction:

The CIESIN dataset was used to label a sub-grid as 'urban' if the population density exceeds 600/km², and 'rural' otherwise. The urban area fraction (f_{UA}) is then the number of urban sub-grids per native gridcell divided by 576, the total number of sub-grids. The urban population fraction (f_{UP}) is defined as the fraction of the population within the 1°x1° gridcell which resides in the urban-flagged sub-grids.

The GEA population data set provides the urban population fraction g_{UP} within each subgridcell. For each 1°x1° gridcell, we define the urban area fraction f_{UA} and urban population fraction f_{UP} as follows:

[1] Since 2017 an update to GWPv4 is available with projection to 2020, accessible at https://earthdata.nasa.gov/.

$$f_{UA} = \frac{\sum_{i=1}^{64} g_{UP,i} A_i}{\sum_{i=1}^{64} A_i}$$

$$f_{UP} = \frac{\sum_{i=1}^{64} g_{UP,i} POP_i}{\sum_{i=1}^{64} POP_i}$$

Where *i* runs over all 64 population subgrids, with A_i the surface area and POP_i the population number in a subgridcell. The urban area fraction is estimated as the area-weighted average urban population fraction over the 64 sub-grids. This method is less accurate than the CIESIN method and tends to overestimate the urban area fraction and, hence, to smooth out emission and concentration gradients.

Urban increment parameterisation development

We first assume that only a fraction of emitted primary BC and POM is incremented in urban areas, namely only BC and POM emitted from residential and road transport sectors:

$PM_{2.5,inc} = SO_4 + NO_3 + NH_4 + (1\text{-}k_{BC})\ BC + (1\text{-}k_{POM})\ POM + INCR(k_{BC}\ BC + k_{POM}\ POM)$

with SO_4, NO_3, NH_3, BC and POM the 1°x1° gridcell average values resulting from TM5 or TM5-FASST; k_{BC} (k_{POM}) = fraction of (residential + transport) BC (POM) emissions in the total BC (POM) emissions within the 1°x1° gridcell respectively and *INCR* the urban increment factor.

We assume that black carbon anthropogenic emissions E_{BC} in the native gridcell with area A are divided between the urban and rural areas according to their corresponding population fraction. In this way fraction $f_{UP}.E_{BC}$ is emitted from area $f_{UA}.A$ and, to ensure mass conservation, the remaining fraction $(1- f_{UP})E_{BC}$ is emitted from area $(1- f_{UA})A$.

Assuming steady-state conditions and neglecting the incoming concentration of BC from neighbouring gridcells, the 1°x1° grid-average BC concentration can be written as: $C_{BC,1x1} = \frac{E_{BC}}{\lambda}$, with λ the ventilation factor. We assume that this definition of factor λ is also valid for the urban and rural parts of the gridcell, i.e., it is equivalent with the hypothesis that mixing layer height and wind speed are the same. Hence, the steady-state concentration in the urban sub-area can be written as: $C_{BC} = \frac{f_{UP}}{f_{UA}} \cdot \frac{E_{BC}}{\lambda}$ for the urban contribution and $C_{BC} = \frac{(1 - f_{UP})}{(1 - f_{UA})} \cdot \frac{E_{BC}}{\lambda}$ for the rural fraction. The ventilation factor λ, including an implicit correction factor

for the non-zero background concentration in neighbouring cells, is obtained from the explicitly modelled gridcell concentration $C_{BC,TM5}$ as $\lambda = \frac{E_{BC}}{C_{BC,TM5}}$. Hence, the urban enhanced BC concentration within a gridcell is estimated from

$$C_{BC,URB} = \frac{f_{UP}}{f_{UA}} \cdot C_{BC,TM5} \quad [4.1]$$

From the constraint that $f_{UA} \cdot C_{URB} + (1 - f_{UA}) \cdot C_{RUR} = C_{TM5}$ the remaining rural fraction is given by

$$C_{BC,RUR} = \frac{(1 - f_{UP})}{(1 - f_{UA})} \cdot C_{BC,TM5} \quad [4.2]$$

In order to avoid potential artificial spikes in urban concentrations when occasionally a very small fraction of the native gridcell contains a very large fraction of the population, empirical bounds are applied on the adjustment factors: rural primary BC and POM should not be lower than 0.5 times the TM5 grid average, and urban primary BC and POM should not exceed the rural concentration by a factor 5.

After replacing $C_{BC,URB}$ and $C_{BC,RUR}$, the population-weighted concentration is expressed as a correction factor to be applied on the original 1°x1° gridcell mean concentration:

$$C^{pop}_{BC,TM5} = INCR \cdot C^{area}_{BC,TM5} \quad [4.3]$$

Where $$INCR = \left[\frac{(f_{UP})^2}{f_{UA}} + \frac{(1-f_{UP})^2}{1-f_{UA}}\right] \quad [4.4]$$

The analogous process is done for primary anthropogenic organic carbon (POM). All secondary components (sulphates, nitrates) and primary natural PM (mineral dust, sea-salt) are assumed to be distributed uniformly over the native 1°x1° gridcell.

Obviously the highest correction factor is found when a large fraction of the population is concentrated in a small urban area inside the gridcell, generating a high sub-grid gradient. Conversely, large urban agglomerations where the urban population is covering most of the native gridcell do not lead to a large correction factor. In other words, the correction factor will be highest for spatially limited and isolated urban settlements within rural surroundings.

Table S4.2 gives regional population-weighted increment factors for BC and POM based on the baseline simulations performed with TM5 for the year 2000, i.e. using year 2000 population (CIESIN GWPv3) and RCP year 2000 gridded emissions.

We evaluate the improvement of including the sub-grid parametrisation in the estimated $PM_{2.5}$ population-weighted regional mean exposure.

We overlay the 1°x1° grid map of urban-increment-corrected TM5-FASST $PM_{2.5}$ concentrations, computed from HTAP year 2010 emission inventory, with a 1°x1° population gridmap (aggregated from CIESIN (2005) which as a native resolution of 2.5'x2.5') to compute population-weighted $PM_{2.5}$ regional averaged values at the level of the 56 defined FASST regions. The latter are compared with regional averaged population-weighted $PM_{2.5}$ values obtained from 0.1°x0.1° resolution satellite-derived $PM_{2.5}$ fields for the year 2010 (van Donkelaar et al., 2016), overlaid with the same CIESIN (2005) population grid map now regridded to 0.1°x0.1° population grid map interpolated from the. The high resolution satellite $PM_{2.5}$ product features the sub-grid gradients approximated with our simplified approach.

Figure S5.1 shows the median and the inter-90%ile range of individual measurements and corresponding modelled $PM_{2.5}$ concentrations in North-America, Europa and China. Modelled values (based on the high resolution CIESIN population maps for 2005) are shown both for the urban-increment parameterization and for the non-adjusted grid average. In general, TM5 grid-averaged concentrations (rightmost values) are underestimating the measured concentrations, and the applied parameterization improves the performance of the model compared to the non-adjusted $PM_{2.5}$ concentration.

Table S4.1 Population datasets properties

Name	Source	Metrics used	Resolution	Nr. of sub-grid per TM5 1°x1° gridcell	Years available
CIESIN[1]	University of Columbia	Population density Population count	2.5'x2.5'	24x24 sub-grids	1990, 2000, 2005
GEA[2]	United Nations population division	Population count Urban population count	7.5'x7.5'	8x8 sub-grids	2000, 2005, 2010, 2020, 2030, … , 2100

[1] CIESIN, 2005

[2] Riahi et al., 2012

Table S4.2 Regional urban increment factors for primary $PM_{2.5}$ from RCP emissions and population for the year 2000.

CNTRY	BC URB INCR FACTOR	POM URB INCR FACTOR	CNTRY	BC URB INCR FACTOR	POM URB INCR FACTOR
AUT	1.90	1.30	RIS	2.28	2.08
CHE	1.72	1.18	RUS	2.43	1.83
BLX	1.84	1.54	RUE	1.75	1.18
ESP	2.46	1.56	UKR	2.07	1.76
FIN	1.98	1.44	COR	1.90	1.88
FRA	2.12	1.36	JPN	1.46	1.65
GBR	1.82	1.51	AUS	2.44	1.54
GRC	2.36	1.71	NZL	1.98	1.50
ITA	2.00	1.49	PAC	1.00	1.00
RFA	1.73	1.43	MON	1.19	1.30
SWE	1.78	1.30	CHN	1.00	1.14
TUR	1.34	1.20	TWN	2.13	2.23
NOR	1.64	1.17	RSAS	1.91	1.72
BGR	1.38	1.12	NDE	2.00	1.75
HUN	1.56	1.23	IDN	1.13	1.09
POL	1.61	1.33	THA	1.00	1.05
RCEU	1.11	1.04	MYS	1.72	1.64
RCZ	1.49	1.22	PHL	1.08	1.17
ROM	1.30	1.15	VNM	1.00	1.09
MEME	2.02	1.71	RSEA	1.00	1.03
NOA	1.34	1.55	CAN	2.05	1.77
EGY	2.34	1.88	USA	2.00	1.65
GOLF	2.03	1.59	BRA	1.69	1.50
WAF	1.20	1.15	MEX	1.93	1.63
EAF	1.06	1.04	RCAM	1.57	1.30
SAF	1.07	1.03	CHL	2.15	1.93
RSA	2.00	1.73	ARG	1.63	1.41
KAZ	1.94	1.49	RSAM	1.89	1.51

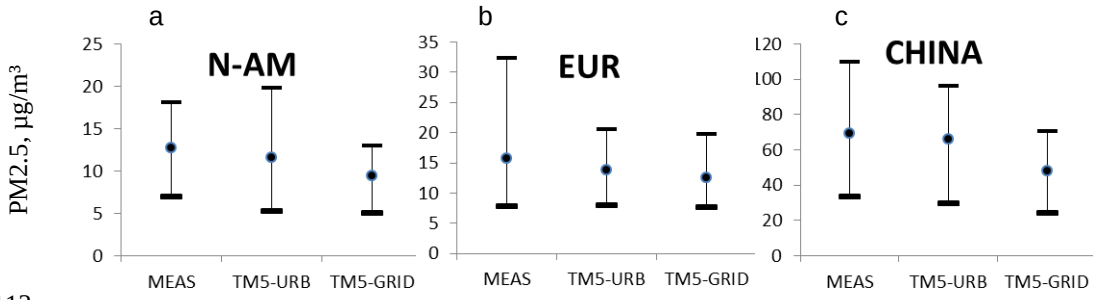

Figure S4.1 Measured and modelled median (and 90% CI) urban $PM_{2.5}$ concentrations in North America (at), Europe (b) and China (c). Measurements are from routine monitoring programs. TM5-URB values include the urban increment correction described in the text, and TM5-GRID refers to the unadjusted gridcell average $PM_{2.5}$ concentrations.

S5 Supplemental information to section 2.5 – Health impacts

S5.1 Sources for population statistics

We use high-resolution population grid maps up to 2100 that were prepared for the Global Energy Assessment (GEA, 2012), based on the Medium Fertility variant of UN population projections (UN DESA, 2009). Year 2030 population distribution by age class, which are required to establish the age classes ≥30 and <5 years are obtained from the United Nations Population Division (2015) Revision. Alternatively the high-resolution Gridded Population of the World V3 (CIESIN, 2005) can be used for scenario years between 2000 and 2015.

S5.2 Baseline mortality rates for relevant causes of death

Cause-specific base mortalities from stroke, ischemic heart disease (IHD), chronic obstructive pulmonary disease (COPD), acute lower respiratory illness diseases (ALRI) and lung cancer (LC) are obtained from WHO (2008)[2]

Cause-specific base mortalities for the year 2005 are taken from the WHO ICD-10 update (WHO, 2012) for individual countries where available, or back-calculated from 14 WHO regional average mortalities when not available. Projections until 2030 are taken from WHO Global Health estimates[3]. In the tool, mortalities for the year 2005 are used for scenario years up till 2005, and mortalities for the year 2030 are used for scenario years 2030 and beyond. Intermediate years are interpolated.

S5.3 Implementation of Integrated Exposure-Response (IE) functions

The dataset attached to Burnett et al. (2014) contains the outcome of a Monte Carlo analysis with an ensemble of 1000 fitted values of the parameters α, β, δ and *zcf* for each of the five health outcomes which is not practical to implement for a fast screening of health impacts. In TM5-FASST_v0 we implement the IER data set as analytical functions, immediately providing RR($PM_{2.5}$) as well as the 95% CI. For simplicity we implemented the all-age functions for each health outcome, although the Burnett et al. data set contains as well age-specific fittings for IHD and stroke.

We generate an array of $PM_{2.5}$ values between 0 and 300µg/m³ and calculate for each value 1000 RRs using the corresponding 1000 function parameter sets, from which we derive for each $PM_{2.5}$ value the median and 95%

[2] http://www.who.int/healthinfo/global_burden_disease/cod_2008_sources_methods.pdf

[3] http://www.who.int/healthinfo/global_burden_disease/en/

RR. Next we make a fitting of the resulting median and 95% CI RR($PM_{2.5}$), using the proposed functional shape for the IER functions.

$$RR(PM_{2.5}) = 1 + \alpha \left[1 - e^{-\gamma(PM2.5-zcf)^{\delta}}\right]$$

The generated RR ($PM_{2.5}$) and best fit analytical functions are shown in Fig. A6, and the corresponding parameter values are given in Table S6. It is important to note that the resulting best fit parameter values to the median and 95% of RR($PM_{2.5}$) do not coincide with the median and 95% CI of the Monte Carlo ensemble of 1000 respective parameters.

Table S5 IER fitted function parameters (parameters have been fitted to a range up to 300 µg/m³)

	COPD	LC	ALRI	STROKE	IHD
			MEDIAN		
α	58.99	54.61	1.98	1.03	0.83
β	0.00031	0.00034	0.00259	0.02002	0.07101
δ	0.67	0.74	1.24	1.07	0.55
zcf	7.58	6.91	6.79	8.80	6.86
			2.5%ile		
α	28.91	12.54	1.61	1.35	1.02
β	0.00015	0.00013	0.01025	0.02064	0.05557
δ	0.83	1.02	0.81	0.49	0.40
zcf	8.19	7.24	13.84	10.91	9.62
			97.5%ile		
α	120.48	23.51	2.82	1.41	1.21
β	0.00028	0.00169	0.00083	0.01469	0.01283
δ	0.63	0.67	1.50	1.26	1.09
zcf	6.02	6.56	1.50	7.21	1.97

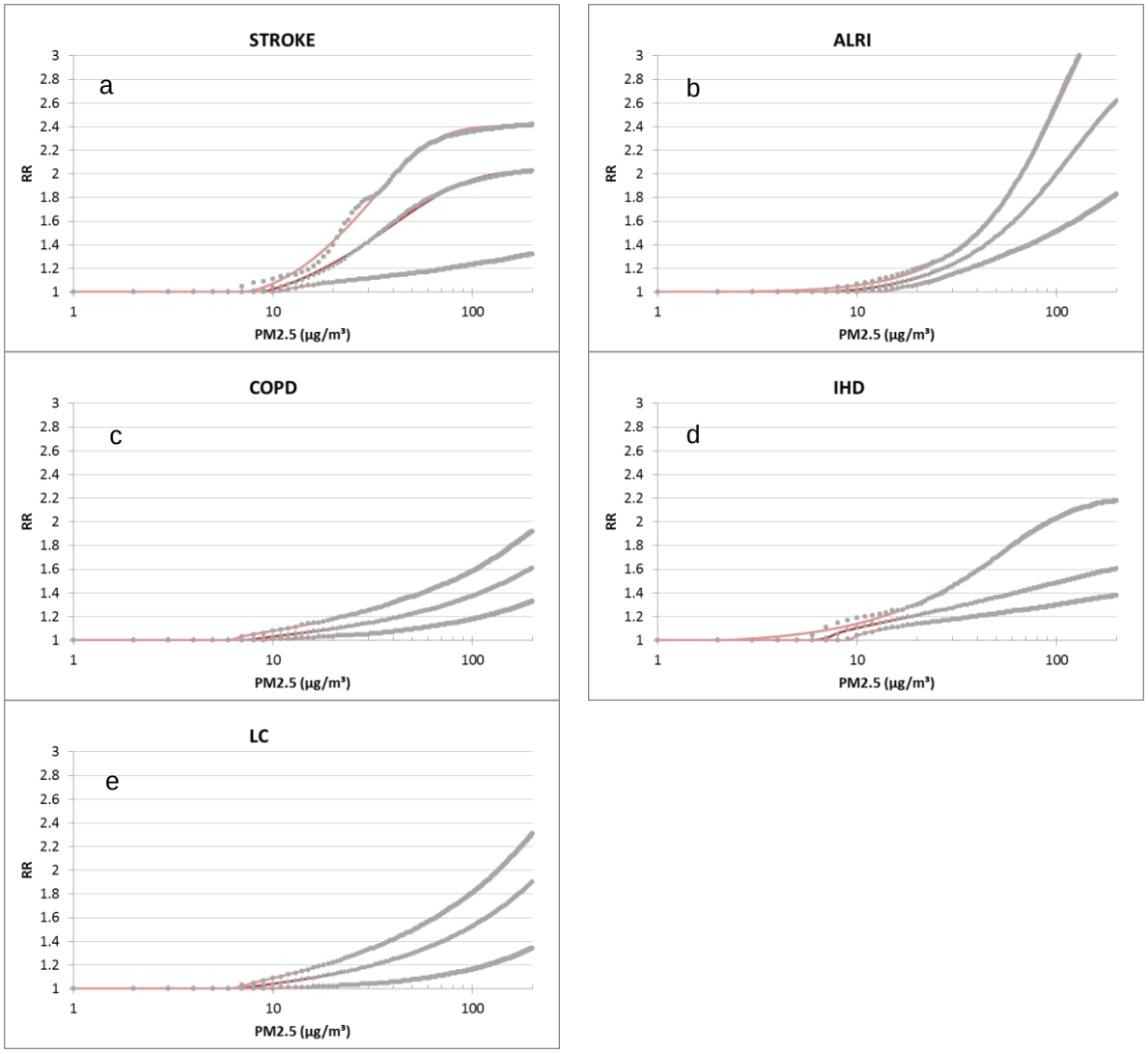

Figure S5: Dashed line: Median and 95% CI of the relative risk (RR) as a function of exposure to $PM_{2.5}$ from 1000 Monte Carlo samples provided by Burnett et al. (2014). Red lines: fitted curves for all-age IER functions for 5 mortality causes, using the parameters listed in Table S6.1 (this work). (a): Stroke, (b): Acute Lower Respiratory Airways Infections (c) Chronic Obstructive Pulmonary Disease (d) Ischemaic Heart Disease (e) Lung Cancer

S6 Supplemental information to section 2.7 – Climate metrics

S6.1 calculation of aerosol optical properties and radiative forcing in TM5

The broadband aerosol optical properties were determined in two steps: first, the spectral optical properties in the wavelength region between 0.2 μm and 5 μm were calculated on the basis of Mie theory. Only the short-to-infrared wave spectrum 0.2-5 μm has been considered, since the anthropogenic aerosols are most efficient in scattering and absorbing the solar radiation in the submicron size range. In a second step, these spectral quantities were weighted by the extra-terrestrial solar flux (Wehrli, 1985), and averaged over the applied wavelength intervals of the Off-line Radiative Transfer Model (ORTM).

TM5 determines aerosol mass, and does not provide information about particle size distributions or particle densities, so assumptions were made about these properties for the Mie calculations (Table S7.1). We assume a lognormal size distribution with a geometric mean radius r_g of 0.05 μm for inorganics and OC, a geometric standard deviation σ_g of 1.8 for sulphate and 2.0 for OC, and a particle density of 1600 $kg.m^{-3}$ and 1200 $kg.m^{-3}$ respectively. The optical properties of inorganics, which mainly scatter shortwave radiation, are reasonably well known compared with other types of aerosols (Li et al., 2001). Wavelength-dependent complex refractive indices for sulphate were taken from Toon et al. (1976). The same values were assumed for organic carbon (Lund Myhre and Nielsen, 2004; Sloane, 1983). The geometric mean radius for BC particles is assumed to be 0.0118 mm with a sigma of 2.0 and a particle density of 1800 $kg.m^{-3}$ (Penner et al., 1998). For the BC refractive indices, the values from Fenn et al. (1985) were applied. We assume externally mixed aerosols and calculate the forcing separately for each component. The total aerosol forcing is obtained by summing up these contributions.

The aerosol water content is calculated assuming equilibrium between aerosol particles and atmospheric water vapour pressure at each location. The modification of aerosol specific extinction due to relative humidity of the ambient air is considered using a simple approximation adapted from the data given by Nemesure et al. (1995). For relative humidities (RH) below 80%, the specific extinction is enhanced by a factor of RH*0.04, assuming a minimum RH of 25%. For RH exceeding 80%, the specific extinction increases exponentially with RH. The factor 9.9 is reached for RH = 100%. Exponential growth is assumed for hygroscopic aerosols (ammonium salts and organic carbon). Black carbon (here assumed to be externally mixed) is assumed to be mostly hydrophobic and its specific extinction increases only linearly with RH. Single scattering albedo and the asymmetry factor are assumed to be independent of RH. This approach might result in a small overestimation of the shortwave radiative forcing of scattering aerosols, because with increasing relative humidity forward scattering is increased and backscattering in space direction reduced (asymmetry factor increased).

187 **Table S6.1 Parameters of aerosol log-normal size distributions**

	r_g (μm)	σ_g	Density (kg m^{-3})	Refr. index real	Refr. index imaginary
Inorganic	0.05	1.8	1600	1.53	$1.0x10^{-7}$
BC	0.0118	2.0	1800	1.75	$4.4x10^{-1}$
OC	0.05	2.0	1200	1.53	$1.0x10^{-7}$

188
189

S6.2 Tables with emission-based forcing efficiencies by source region in TM5-FASST

Table S6.2 Regional emission-to-global forcing efficiencies for aerosol precursors (no feedback on O_3 included)

		DIRECT				INDIRECT	
FASST REGION	FASST CODE	W/m^2/Tg SO_2	W/m^2/Tg NO_x	W/m^2/Tg BC	W/m^2/Tg POM	W/m^2/Tg NH_3	W/m^2/Tg SO_2
N-AFR	NOA	-7.38E-03	-8.13E-04	5.32E-02	-1.28E-02	-0.00426	-7.19E-03
W-AFR	WAF	-6.74E-03	-2.91E-04	3.02E-02	-1.01E-02	-0.00242	-1.14E-02
E-AFR	EAF	-9.41E-03	-9.07E-04	3.22E-02	-9.92E-03	-0.00473	-1.69E-02
S-AFR	SAF	-8.74E-03	-1.21E-03	3.07E-02	-1.10E-02	-0.00495	-2.57E-02
REP. S. AFR	RSA	-4.03E-03	-4.24E-04	1.64E-02	-5.55E-03	-2.32E-03	-1.98E-02
AUSTRALIA	AUS	-4.20E-03	-1.03E-04	2.02E-02	-6.63E-03	-2.18E-03	-2.06E-02
NZL	NZL	-1.84E-03	-1.03E-04	8.12E-03	-2.84E-03	-1.25E-03	-2.42E-02
S KOREA	COR	-1.66E-03	-6.80E-05	1.20E-02	-4.69E-03	-3.14E-03	-3.36E-03
JAPAN	JPN	-1.45E-03	-9.75E-05	9.59E-03	-2.85E-03	-1.16E-03	-4.25E-03
MON+N KOREA	MON	-1.89E-03	-4.48E-04	1.47E-02	-5.24E-03	-1.77E-03	-3.70E-03
CHINA	CHN	-2.18E-03	-4.41E-04	1.67E-02	-4.93E-03	-2.24E-03	-4.90E-03
TWN	TWN	-2.48E-03	-3.75E-05	8.51E-03	-3.14E-03	-2.13E-03	-6.94E-03
AUT+SLV	AUT	-3.23E-03	-3.66E-04	2.45E-02	-6.03E-03	-2.21E-03	-3.03E-03
SWITZERLAND	CHE	-3.15E-03	-3.73E-04	2.39E-02	-5.74E-03	-2.70E-03	-3.07E-03
BE+NL+LUX	BLX	-1.63E-03	-3.43E-04	1.36E-02	-3.72E-03	-2.46E-03	-2.14E-03
SP+POR	ESP	-5.06E-03	-4.68E-04	2.82E-02	-8.58E-03	-3.25E-03	-5.31E-03
FIN	FIN	-1.38E-03	-1.18E-04	1.84E-02	-3.33E-03	-1.40E-03	-1.35E-03
FRA	FRA	-2.75E-03	-3.91E-04	1.87E-02	-5.56E-03	-1.88E-03	-3.30E-03
GBR+IRL	GBR	-1.52E-03	-1.70E-04	1.21E-02	-3.66E-03	-1.82E-03	-3.45E-03
GRC+CYP	GRC	-4.66E-03	-8.43E-04	3.87E-02	-9.11E-03	-2.64E-03	-3.91E-03
ITA+MLT	ITA	-3.97E-03	-5.40E-04	2.88E-02	-7.93E-03	-2.37E-03	-3.42E-03
GER	RFA	-2.16E-03	-4.24E-04	1.72E-02	-4.38E-03	-2.33E-03	-2.46E-03
SWE+DK	SWE	-1.47E-03	-3.77E-04	1.53E-02	-3.56E-03	-1.15E-03	-1.80E-03
NORWAY	NOR	-1.47E-03	-2.16E-04	1.67E-02	-3.07E-03	-6.27E-04	-4.59E-03
BULGARIA	BGR	-3.90E-03	-7.18E-04	3.27E-02	-7.59E-03	-2.36E-03	-3.13E-03

(continues on next page)

Table S6.2 Cont'd

FASST REGION	FASST CODE	DIRECT				INDIRECT	
		$W/m^2/Tg$ SO_2	$W/m^2/Tg$ NO_x	$W/m^2/Tg$ BC	$W/m^2/Tg$ POM	$W/m^2/Tg$ NH_3	$W/m^2/Tg$ SO_2
HUN	HUN	-2.91E-03	-3.39E-04	2.35E-02	-5.39E-03	-2.23E-03	-2.88E-03
POL+BALTIC	POL	-1.96E-03	-2.01E-04	1.75E-02	-3.66E-03	-1.66E-03	-2.47E-03
REST OF C EUR	RCEU	-3.58E-03	-6.60E-04	3.07E-02	-7.30E-03	-1.69E-03	-3.23E-03
CZ+SLK	RCZ	-2.47E-03	-3.13E-04	2.14E-02	-4.90E-03	-2.46E-03	-2.63E-03
ROM	ROM	-3.13E-03	-4.83E-04	2.47E-02	-5.84E-03	-2.02E-03	-2.61E-03
MEX	MEX	-6.35E-03	-3.03E-04	1.97E-02	-7.89E-03	-3.36E-03	-1.38E-02
REST OF C AM	RCAM	-3.93E-03	-3.96E-04	1.53E-02	-6.57E-03	-1.90E-03	-1.01E-02
MIDDLE EAST	MEME	-4.83E-03	-1.49E-03	4.29E-02	-9.49E-03	-3.33E-03	-4.70E-03
EGY	EGY	-5.73E-03	-5.21E-04	5.64E-02	-1.21E-02	-2.93E-03	-6.05E-03
GULF REGION	GLF	-7.14E-03	-1.49E-03	4.40E-02	-1.08E-02	-1.61E-03	-7.80E-03
TUR	TUR	-4.76E-03	-4.83E-04	3.55E-02	-8.01E-03	-2.92E-03	-4.18E-03
CANADA	CAN	-1.80E-03	-2.87E-04	1.96E-02	-3.35E-03	-1.91E-03	-4.16E-03
USA	USA	-2.84E-03	-1.33E-04	1.69E-02	-5.55E-03	-2.67E-03	-5.79E-03
PAC	PAC	-3.25E-03	-1.03E-04	9.01E-03	-2.72E-03	-1.44E-03	-1.74E-02
KAZ	KAZ	-2.31E-03	-4.89E-04	2.90E-02	-4.36E-03	-2.15E-03	-4.14E-03
FRMR USSR AS	RIS	-2.83E-03	-2.56E-04	2.79E-02	-4.93E-03	-2.51E-03	-4.50E-03
RUS-EUR	RUS	-2.47E-03	-2.10E-04	2.44E-02	-4.24E-03	-1.76E-03	-3.22E-03
RUS-ASIA	RUE	-2.15E-03	-7.52E-04	2.58E-02	-3.91E-03	-1.12E-03	-3.90E-03
UKR	UKR	-2.78E-03	-3.61E-04	2.33E-02	-5.04E-03	-1.92E-03	-3.07E-03
BRAZIL	BRA	-5.21E-03	-1.77E-04	2.00E-02	-7.40E-03	-1.58E-03	-1.30E-02
CHL	CHL	-4.88E-03	-4.26E-04	2.15E-02	-6.74E-03	-1.66E-03	-2.38E-02
ARG	ARG	-8.75E-04	-4.26E-04	1.32E-02	-4.51E-03	-8.03E-04	-1.52E-02
REST OF S AM	RSAM	-5.31E-03	-9.85E-05	1.50E-02	-5.10E-03	-1.57E-03	-1.31E-02
REST OF S AS	RSAS	-6.46E-03	-1.41E-04	3.02E-02	-9.09E-03	-1.73E-03	-8.34E-03

(continues on next page)

197 **Table S6.2 Cont'd**

FASST REGION	FASST CODE	DIRECT				INDIRECT	
		$W/m^2/Tg$ SO_2	$W/m^2/Tg$ NO_x	$W/m^2/Tg$ BC	$W/m^2/Tg$ POM	$W/m^2/Tg$ NH_3	$W/m^2/Tg$ SO_2
INDIA	NDE	-6.29E-03	-1.41E-04	2.61E-02	-9.37E-03	-1.59E-03	-9.66E-03
INDON	IDN	-3.65E-03	-4.41E-04	1.17E-02	-4.35E-03	-6.19E-04	-1.89E-02
THAIL	THA	-3.78E-03	-4.41E-04	1.45E-02	-5.37E-03	-1.08E-03	-1.19E-02
MALYS	MYS	-3.14E-03	-4.41E-04	1.32E-02	-5.02E-03	-1.16E-03	-2.63E-02
PHIL	PHL	-2.64E-03	-4.41E-04	8.79E-03	-3.44E-03	-1.47E-03	-1.56E-02
VTNAM	VNM	-2.90E-03	-4.41E-04	1.30E-02	-5.02E-03	-1.19E-03	-1.13E-02
REST OF EAS	RSEA	-6.16E-03	-4.41E-04	1.81E-02	-7.83E-03	-1.14E-03	-1.40E-02
SHIP	SHIP	-2.32E-03	-8.95E-05	1.26E-02	-2.06E-03	0.00E+00	-9.38E-03

198

Table S6.3: Global response in radiative forcing due to emissions of CO by including the short and long-term feedback on CH_4 and O_3. S-O_3: short-term O_3 contribution M-O3: long term O_3 forcing feedback via CH_4 lifetime I-CH_4: long-term feedback on CH_4 via CH_4 lifetime

	CO forcing (W/m²/Tg CO)		
	S-O_3	M-O_3	I-CH4
North-America	1.20E-04	3.61E-05	8.78E-05
Europe	6.93E-05	3.95E-05	9.62E-05
South Asia	1.33E-04	4.25E-05	1.04E-04
East Asia	1.08E-04	4.27E-05	1.04E-04
Rest of the World	6.03E-05	4.36E-05	1.06E-04

Table S6.4: Global response in radiative forcing to CH_4 emissions, including the long-term feedback on O_3

	CH_4 forcing (W/m²/Tg CH_4)	
	Direct CH_4	O_3 feedback
Globe	1.79E-03	7.16E-04

Table S6.5 Global response in radiative forcing due to regional emissions of short-lived O_3 precursors - including the long-term feedback on CH_4 and O_3. S-O_3: short-term O_3 contribution M-O3: long term O_3 forcing feedback via CH_4 lifetime I-CH_4: long-term feedback on CH_4 via CH_4 lifetime.

	Forcing (W/m²/Tg NO_2)			Forcing (W/m²/Tg NMVOC)			Forcing (W/m²/Tg SO_2)		
	S-O_3	M-O_3	I-CH4	S-O_3	M-O_3	I-CH4	S-O_3	M-O_3	I-CH4
NOA	1.20E-03	-7.63E-04	-1.86E-03	2.32E-04	1.34E-04	3.26E-04	-1.29E-04	1.28E-05	3.11E-05
WAF	1.42E-03	-9.95E-04	-2.43E-03	2.04E-04	1.26E-04	3.06E-04	-9.05E-05	1.42E-05	3.45E-05
EAF	1.28E-03	-7.96E-04	-1.94E-03	1.90E-04	1.15E-04	2.81E-04	-6.89E-05	1.68E-05	4.09E-05
SAF	1.35E-03	-7.86E-04	-1.92E-03	1.51E-04	1.24E-04	3.02E-04	-1.65E-04	2.41E-05	5.88E-05
RSA	1.27E-03	-6.99E-04	-1.70E-03	3.93E-04	3.56E-05	8.66E-05	-9.92E-05	2.33E-05	5.67E-05
AUS	2.80E-03	-1.48E-03	-3.61E-03	2.55E-04	1.40E-04	3.40E-04	-6.01E-05	1.54E-05	3.75E-05
NZL	2.95E-03	-1.95E-03	-4.77E-03	8.45E-05	1.96E-04	4.76E-04	-6.01E-05	4.11E-07	1.00E-06
COR	3.02E-04	-1.75E-04	-4.26E-04	2.92E-04	3.01E-05	7.33E-05	-2.36E-05	2.33E-06	5.68E-06
JPN	4.64E-04	-2.55E-04	-6.22E-04	2.23E-04	1.16E-04	2.82E-04	-2.18E-05	2.04E-06	4.96E-06
MON	5.36E-04	-2.89E-04	-7.03E-04	-2.77E-04	2.02E-04	4.92E-04	-2.25E-05	1.10E-06	2.69E-06
CHN	8.31E-04	-3.66E-04	-8.91E-04	2.11E-04	1.16E-04	2.82E-04	-2.22E-05	4.73E-05	1.15E-04
TWN	1.12E-03	-5.46E-04	-1.33E-03	3.49E-04	7.88E-05	1.92E-04	-4.08E-05	1.40E-06	3.41E-06
AUT	2.54E-04	-1.60E-04	-3.89E-04	2.19E-04	1.12E-04	2.74E-04	-4.23E-05	7.20E-07	1.75E-06
CHE	3.36E-04	-1.89E-04	-4.60E-04	2.22E-04	1.18E-04	2.86E-04	-2.65E-05	1.27E-07	3.10E-07
BLX	8.16E-05	-7.31E-05	-1.78E-04	2.01E-04	1.20E-04	2.91E-04	-1.76E-05	4.66E-07	1.14E-06
ESP	4.89E-04	-3.01E-04	-7.32E-04	2.22E-04	1.14E-04	2.77E-04	-6.54E-05	1.56E-05	3.80E-05
FIN	1.57E-04	-1.40E-04	-3.40E-04	1.60E-04	1.18E-04	2.87E-04	-1.30E-05	1.69E-07	4.13E-07
FRA	2.46E-04	-1.59E-04	-3.87E-04	2.14E-04	1.15E-04	2.79E-04	-3.69E-05	2.50E-06	6.09E-06
GBR	7.17E-05	-8.03E-05	-1.95E-04	2.01E-04	1.22E-04	2.96E-04	-1.69E-05	2.63E-06	6.40E-06
GRC	4.74E-04	-2.87E-04	-7.00E-04	2.70E-04	4.62E-05	1.13E-04	-7.23E-05	5.13E-06	1.25E-05
ITA	3.58E-04	-2.04E-04	-4.97E-04	2.46E-04	8.61E-05	2.10E-04	-5.68E-05	5.76E-06	1.40E-05
RFA	1.29E-04	-9.65E-05	-2.35E-04	1.98E-04	1.17E-04	2.84E-04	-2.28E-05	1.82E-06	4.44E-06
SWE	1.94E-04	-1.60E-04	-3.90E-04	1.60E-04	1.17E-04	2.84E-04	-1.17E-05	2.12E-07	5.16E-07
NOR	4.20E-04	-3.01E-04	-7.33E-04	1.35E-04	1.03E-04	2.50E-04	-1.38E-05	9.75E-07	2.37E-06
BGR	3.63E-04	-2.24E-04	-5.46E-04	2.39E-04	9.99E-05	2.43E-04	-5.05E-05	6.36E-06	1.55E-05

Table S6.5 – Cont'd

	Forcing (W/m²/Tg NO_2)			Forcing (W/m²/Tg NMVOC)			Forcing (W/m²/Tg SO_2)		
	S-O_3	M-O_3	I-CH4	S-O_3	M-O_3	I-CH4	S-O_3	M-O_3	I-CH4
HUN	2.14E-04	-1.42E-04	-3.46E-04	2.07E-04	1.17E-04	2.84E-04	-3.39E-05	1.95E-06	4.75E-06
POL	1.67E-04	-1.20E-04	-2.92E-04	1.93E-04	1.10E-04	2.67E-04	-2.16E-05	4.41E-06	1.07E-05
RCEU	4.17E-04	-2.47E-04	-6.02E-04	2.00E-04	1.24E-04	3.01E-04	-4.56E-05	6.86E-06	1.67E-05
RCZ	1.72E-04	-1.21E-04	-2.95E-04	2.05E-04	1.09E-04	2.66E-04	-2.78E-05	1.27E-06	3.10E-06
ROM	2.52E-04	-1.44E-04	-3.51E-04	2.15E-04	1.17E-04	2.86E-04	-3.63E-05	2.16E-06	5.26E-06
EUR	2.37E-04	-1.59E-04	-3.87E-04	2.01E-04	1.54E-05	3.74E-05	-3.98E-05	5.90E-05	1.44E-04
MEX	1.67E-03	-8.98E-04	-2.19E-03	2.38E-04	1.17E-04	2.84E-04	-9.34E-05	3.15E-05	7.67E-05
RCAM	2.12E-03	-1.22E-03	-2.97E-03	2.08E-04	1.43E-04	3.49E-04	-5.67E-05	5.69E-06	1.39E-05
MEME	5.71E-04	-3.17E-04	-7.72E-04	2.73E-04	1.00E-04	2.44E-04	-1.06E-04	1.05E-05	2.55E-05
EGY	7.14E-04	-4.89E-04	-1.19E-03	3.28E-04	6.19E-05	1.51E-04	-1.13E-04	7.85E-06	1.91E-05
GOLF	1.28E-03	-7.11E-04	-1.73E-03	2.03E-04	1.47E-04	3.59E-04	-1.18E-04	7.70E-05	1.87E-04
TUR	5.69E-04	-3.07E-04	-7.48E-04	2.53E-04	1.01E-04	2.46E-04	-8.00E-05	1.52E-05	3.71E-05
CAN	4.83E-04	-2.85E-04	-6.94E-04	1.39E-04	1.32E-04	3.22E-04	-3.13E-05	8.27E-06	2.01E-05
USA	4.72E-04	-2.39E-04	-5.81E-04	2.35E-04	1.09E-04	2.66E-04	-5.73E-05	8.43E-05	2.05E-04
PAC	4.91E-03	-2.33E-03	-5.69E-03	1.50E-04	1.96E-04	4.77E-04	-4.21E-05	3.75E-07	9.13E-07
KAZ	6.52E-04	-3.36E-04	-8.18E-04	1.57E-04	1.22E-04	2.98E-04	-2.56E-05	5.21E-06	1.27E-05
RIS	7.94E-04	-3.66E-04	-8.93E-04	2.12E-04	1.35E-04	3.28E-04	-4.48E-05	1.48E-06	3.61E-06
RUS	2.93E-04	-1.97E-04	-4.80E-04	1.80E-04	1.26E-04	3.07E-04	-2.16E-05	1.02E-05	2.49E-05
RUE	6.96E-04	-4.02E-04	-9.80E-04	1.11E-04	1.24E-04	3.01E-04	-3.42E-05	5.25E-06	1.28E-05
UKR	2.56E-04	-1.66E-04	-4.04E-04	2.08E-04	1.24E-04	3.03E-04	-3.50E-05	6.48E-06	1.58E-05
BRA	2.84E-03	-1.30E-03	-3.16E-03	8.43E-05	1.41E-04	3.43E-04	-6.90E-05	1.45E-05	3.54E-05
CHL	2.13E-03	-1.30E-03	-3.18E-03	3.06E-04	7.81E-05	1.90E-04	-1.14E-04	1.14E-05	2.77E-05
ARG	2.95E-03	-1.44E-03	-3.52E-03	1.10E-04	1.58E-04	3.84E-04	-1.14E-04	1.93E-06	4.71E-06
RSAM	2.79E-03	-1.52E-03	-3.71E-03	1.33E-04	1.44E-04	3.50E-04	-6.78E-05	7.48E-06	1.82E-05
RSAS	1.20E-03	-5.60E-04	-1.36E-03	2.22E-04	1.32E-04	3.21E-04	-5.08E-05	7.69E-06	1.87E-05
NDE	1.18E-03	-5.97E-04	-1.45E-03	2.59E-04	1.31E-04	3.18E-04	-5.08E-05	4.27E-05	1.04E-04
IDN	2.23E-03	-1.25E-03	-3.05E-03	2.19E-04	1.57E-04	3.83E-04	-4.21E-05	1.01E-05	2.46E-05

210

Table S6.5 – Cont'd

	Forcing (W/m²/Tg NO_2)			Forcing (W/m²/Tg NMVOC)			Forcing (W/m²/Tg SO_2)		
	S-O_3	M-O_3	I-CH4	S-O_3	M-O_3	I-CH4	S-O_3	M-O_3	I-CH4
THA	1.90E-03	-9.83E-04	-2.40E-03	2.22E-04	1.37E-04	3.33E-04	-4.21E-05	4.81E-06	1.17E-05
MYS	2.23E-03	-1.18E-03	-2.87E-03	2.54E-04	1.47E-04	3.59E-04	-4.21E-05	2.36E-06	5.76E-06
PHL	2.29E-03	-1.07E-03	-2.61E-03	3.57E-04	1.57E-04	3.82E-04	-4.21E-05	6.33E-06	1.54E-05
VNM	2.03E-03	-1.04E-03	-2.53E-03	2.14E-04	1.60E-04	3.91E-04	-4.21E-05	9.48E-07	2.31E-06
RSEA	1.40E-03	-8.07E-04	-1.97E-03	1.48E-04	1.40E-04	3.41E-04	-4.21E-05	8.35E-07	2.03E-06
SHIP	1.40E-03	-8.46E-04	-2.06E-03	0.00E+00	0.00E+00	0.00E+00	-2.87E-05	3.64E-05	8.87E-05
AIR	4.25E-03	-1.14E-03	-2.77E-03	0.00E+00	0.00E+00	0.00E+00	0.00E+00	0.00E+00	0.00E+00

211

Table S6.6 Year 2000 global anthropogenic forcing (W/m²) by component from TM5-FASST, versus values reported in AR5 (1750 – 2011). Large scale forest fires have not been included.

		CH_4	BC $PM2_{.5}$	OC $PM_{2.5}$	O_3 (SS)	O_3 (PM)	NO_3 $PM_{2.5}$	SO_4 $PM_{2.5}$	INDIR	TOT
CH_4	AR5	0.641				0.24				0.88
	FASST	*0.500*				*0.20*				*0.70*
CO	AR5	0.072			0.075					0.15
	FASST	*0.083*			*0.074*	*0.034*				*0.19*
NMVOC	AR5	0.025			0.042					0.07
	FASST	*0.049*			*0.033*	*0.020*				*0.10*
NO_x	AR5	-0.245			0.14		-0.040			-0.14
	FASST	*-0.167*			*0.13*	*-0.068*	*-0.040*			*-0.15*
NH_3	AR5						-0.070	0.01		-0.06
	FASST						*-0.091*			*-0.09*
BC	AR5		0.60							0.60
	FASST		*0.15*							*0.15*
OC	AR5			-0.29						-0.29
	FASST			*-0.24*						*-0.24*
SO_2	AR5							-0.41		-0.21
	FASST							*-0.37*		*-0.37*
INDIRECT AEROSOLS	AR5								-0.45	-0.45
	FASST								*-0.81*	*-0.81*

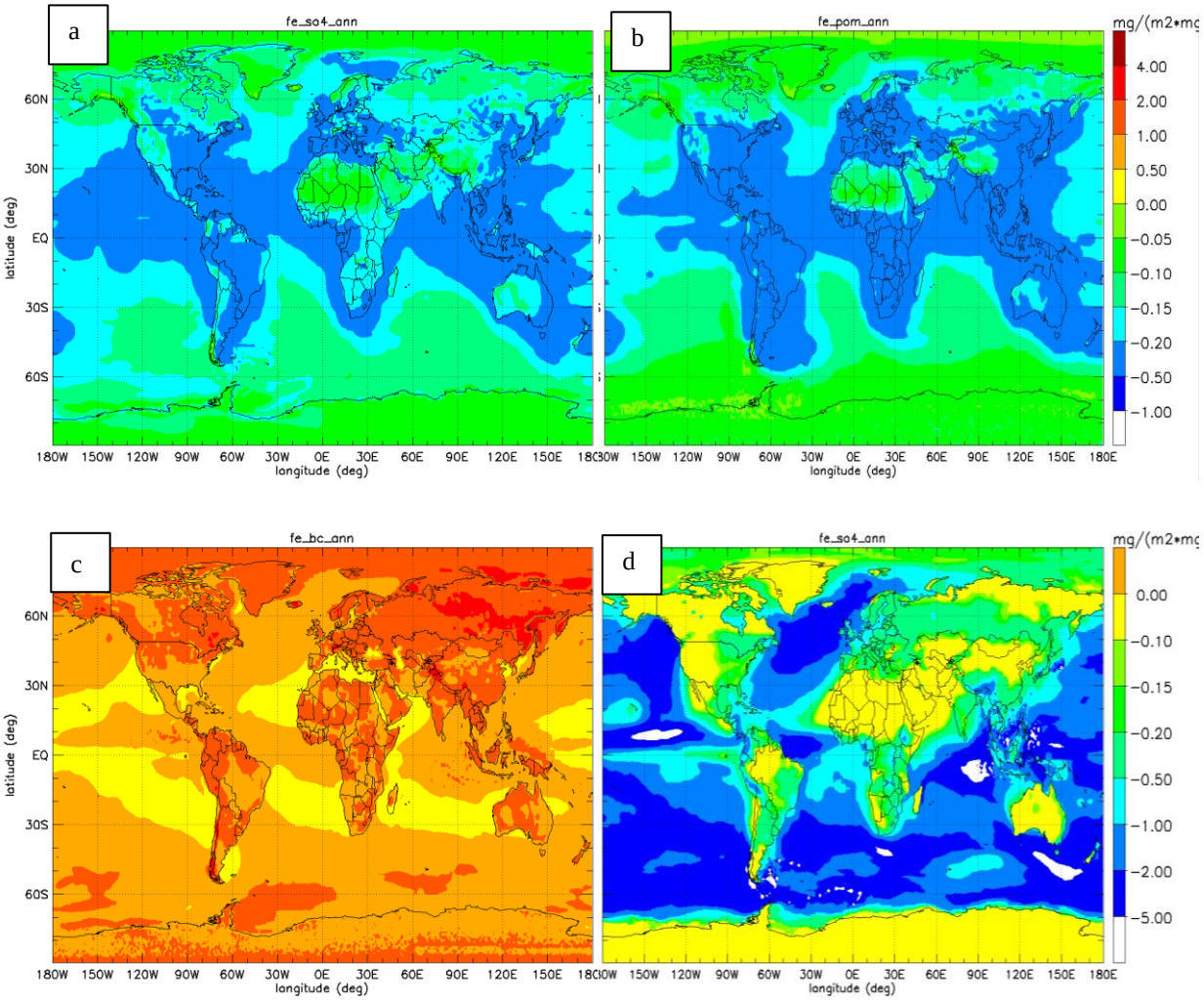

215 **Figure S6.1: Annual average radiative forcing efficiencies for SO4, Particulate Organic Matter, Black carbon, and**
216 **the indirect forcing associated with SO4 [W/(m^2*mg]. a-b-c: direct SO_4, POM, BC (upper legend); d: indirect SO_4**
217 **(lower legend)**

218

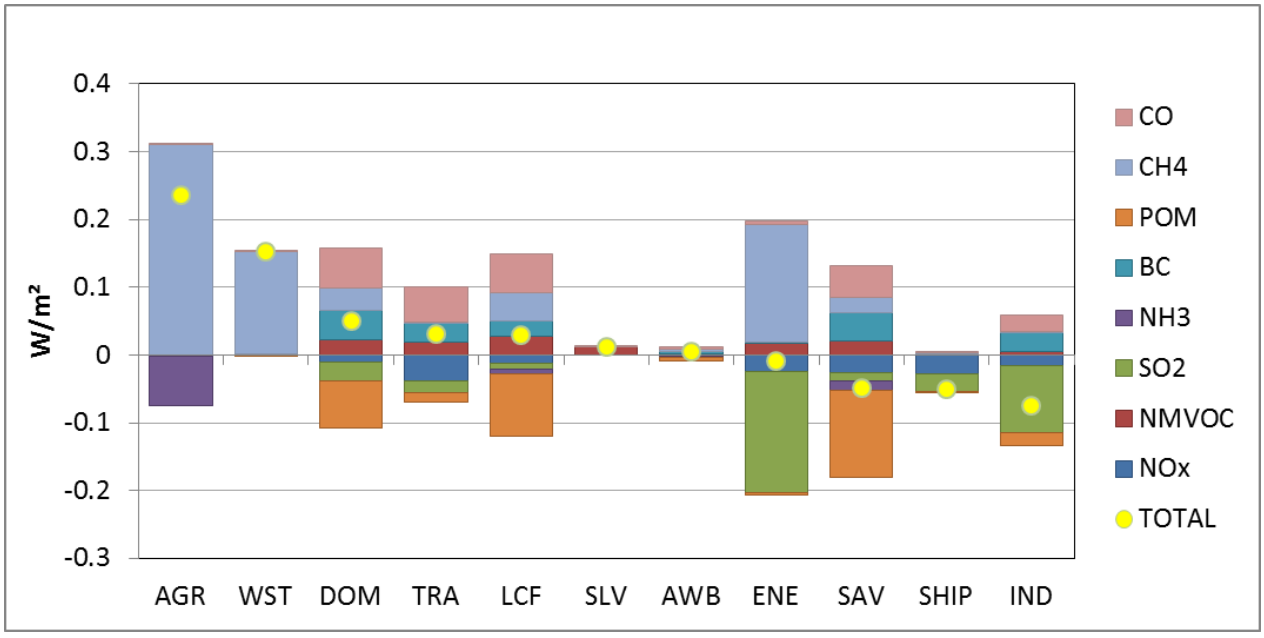

Figure S6.2 TM5-FASST break-down of direct radiative forcing by sector by emitted component, based on RCP year 2000 emission inventory by sector.

S7 Supplemental Figures to section 3.1 - Validation against the full TM5 model: additivity and linearity

PM2.5 additivity of simultaneous SO_2 + NO_x -20% emission perturbation responses

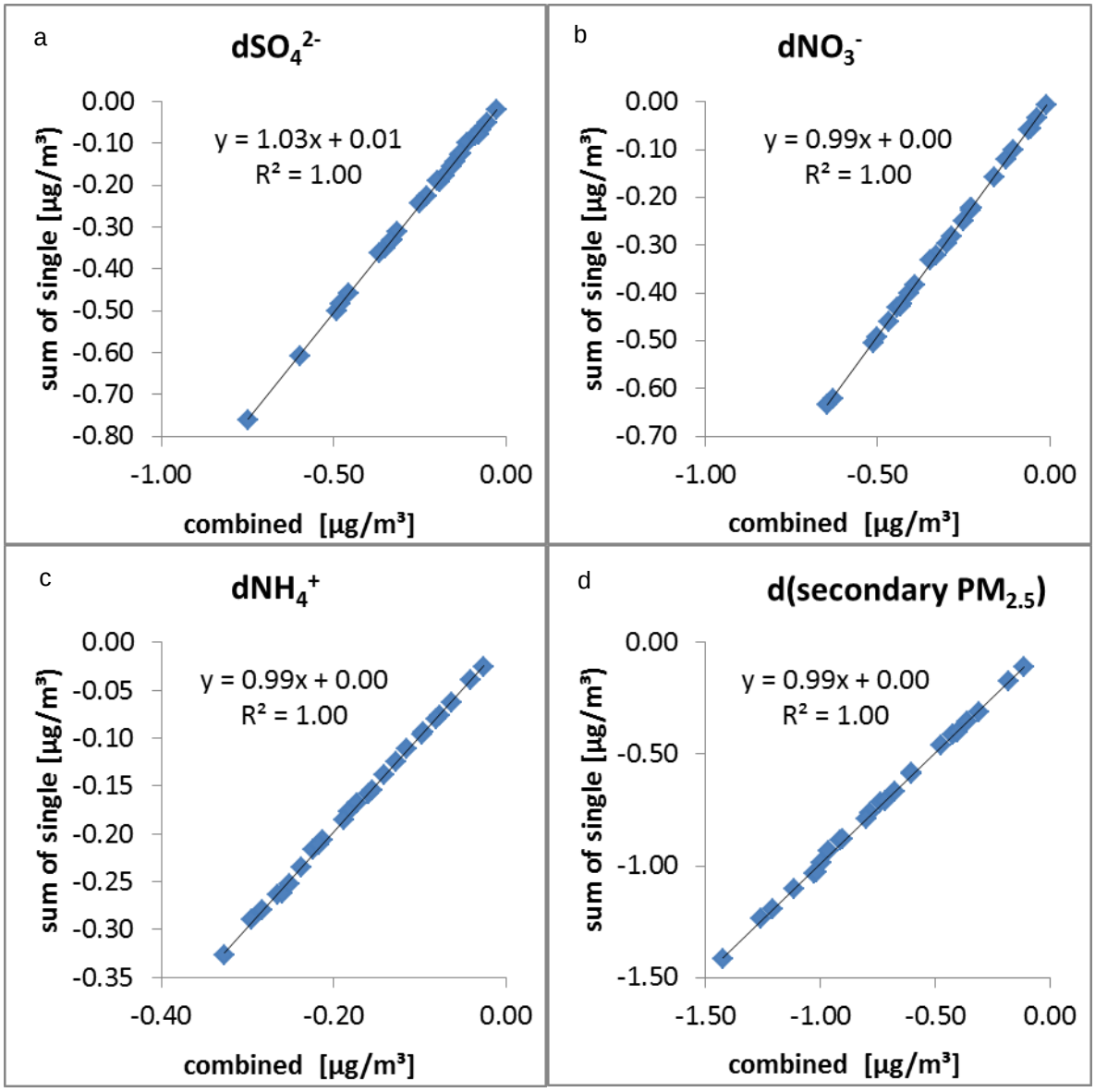

Figure S7.1 Secondary PM2.5 species response to SO_2 and NO_x -20% emission perturbations. Y-axis: summed individual perturbations (P2 + P3) X-axis: response to combined perturbation (P1). All results are obtained with TM5-CTM. (a): sulfate (b) nitrate (c) ammonium (d) sum of all 3 components

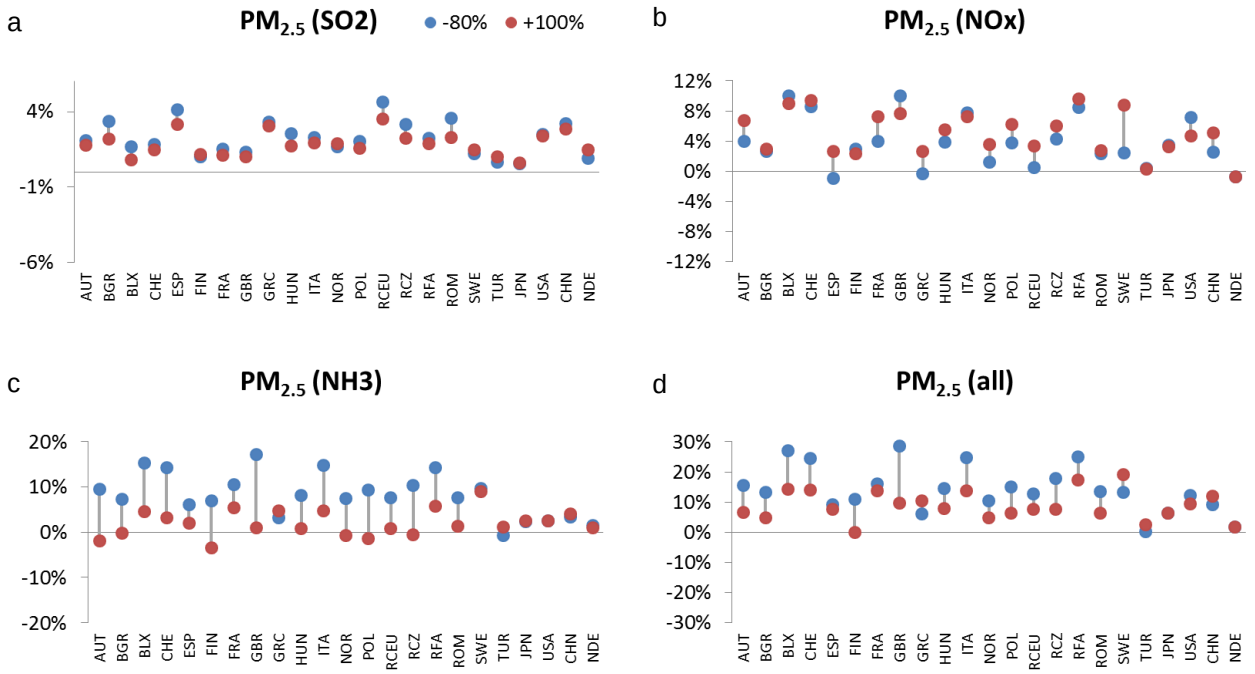

Figure S7.2: Relative error in country/region annual average $PM_{2.5}$ (including primary and secondary components) compared to TM5-CTM by linear extrapolation of a -20% emission perturbation of SO_2 (a), NO_x (b) and NH_3 (c) to -80% (blue dots) and +100% (red dots) respectively for representative source/receptor regions, and the relative error on $PM_{2.5}$ by extrapolation of all 3 precursor emissions simultaneously (d) (as sum of the 3 individual contributions). For the European receptor regions, the perturbation was made over all sub-regions simultaneously.

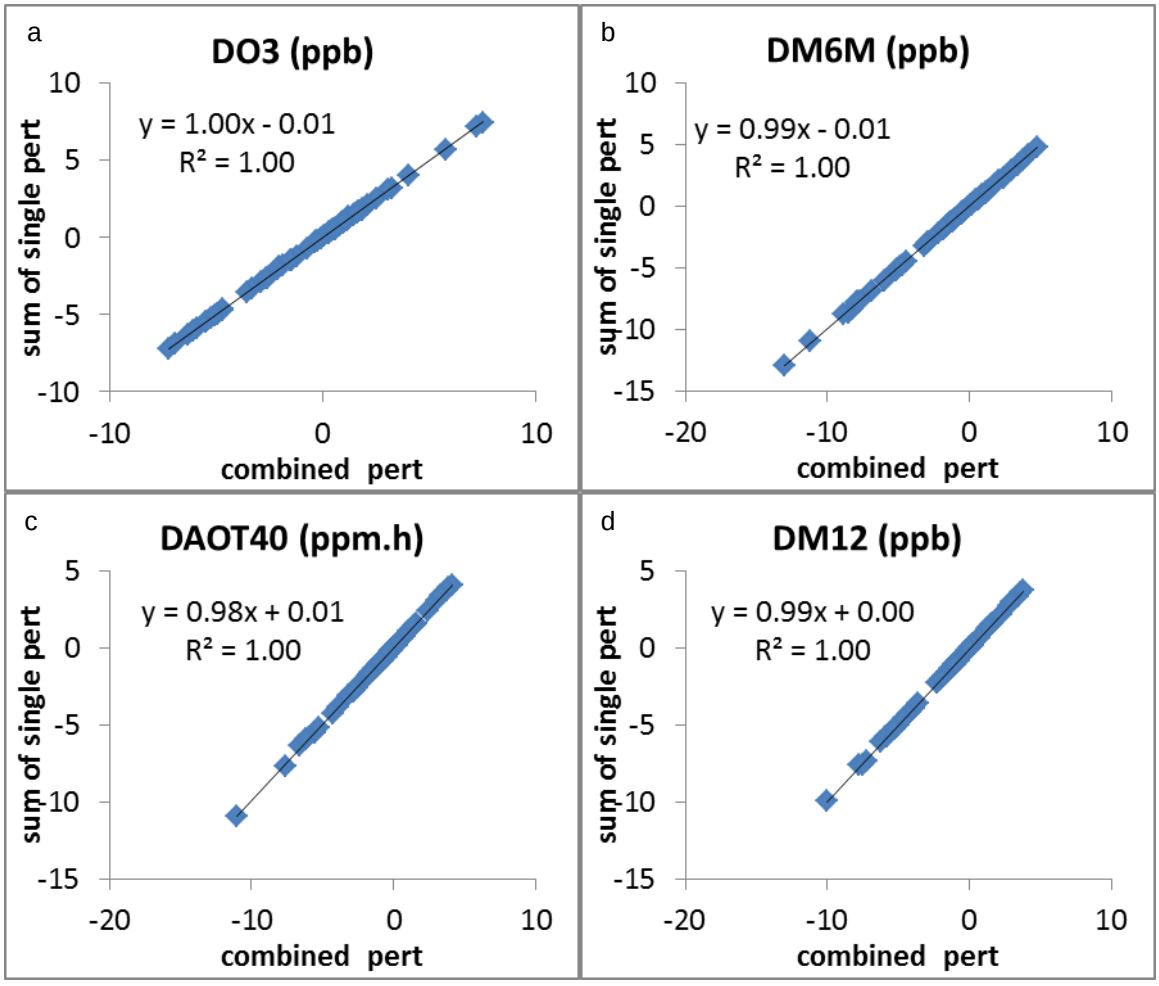

Figure S7.3 TM5 O3 (a) and O3 metrics M6M (b), AOT40 (c) and M12 (d) responses to simultaneous SO_2 and NO_x perturbations including the -80%, -20% and +100% perturbation outcomes for the limited set of source regions. Y-axis: calculated as the sum of the individual responses; X-axis: evaluated from simultaneous perturbation.

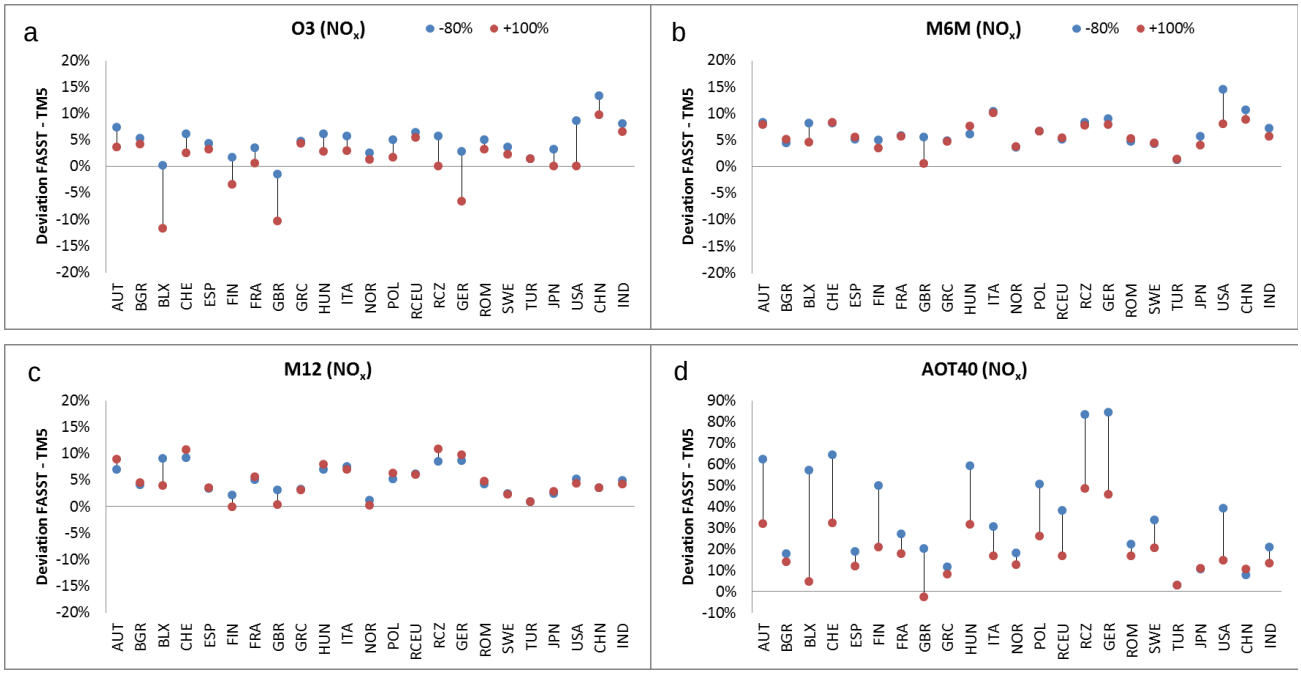

Figure S7.4 Relative error on TM5-FASSST computed (base + perturbation response) annual O_3 (a), and M6M (b), M12 (c), AOT40 (d) exposure metrics relative to TM5 for individual emission perturbations of NO_x of -80% (blue symbols) and +100% (red symbols) relative to the base simulation

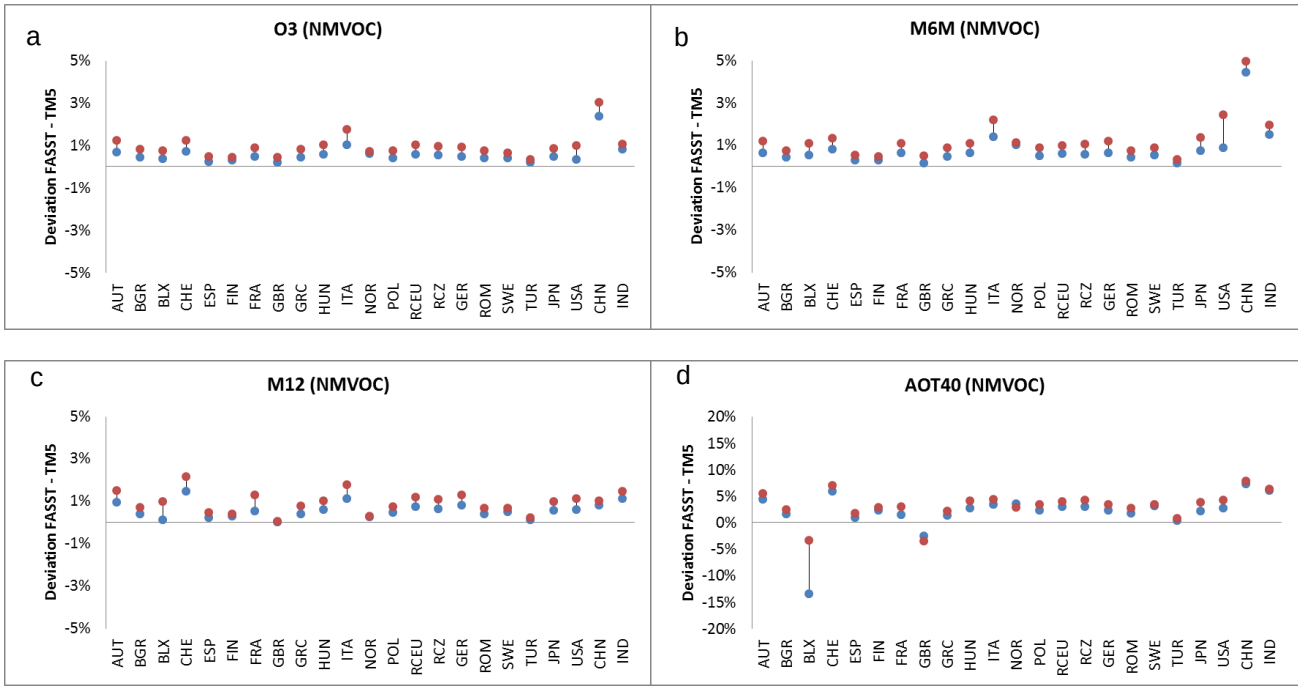

Figure S7.5 Same as Fig S7.4, now for NMVOC perturbations

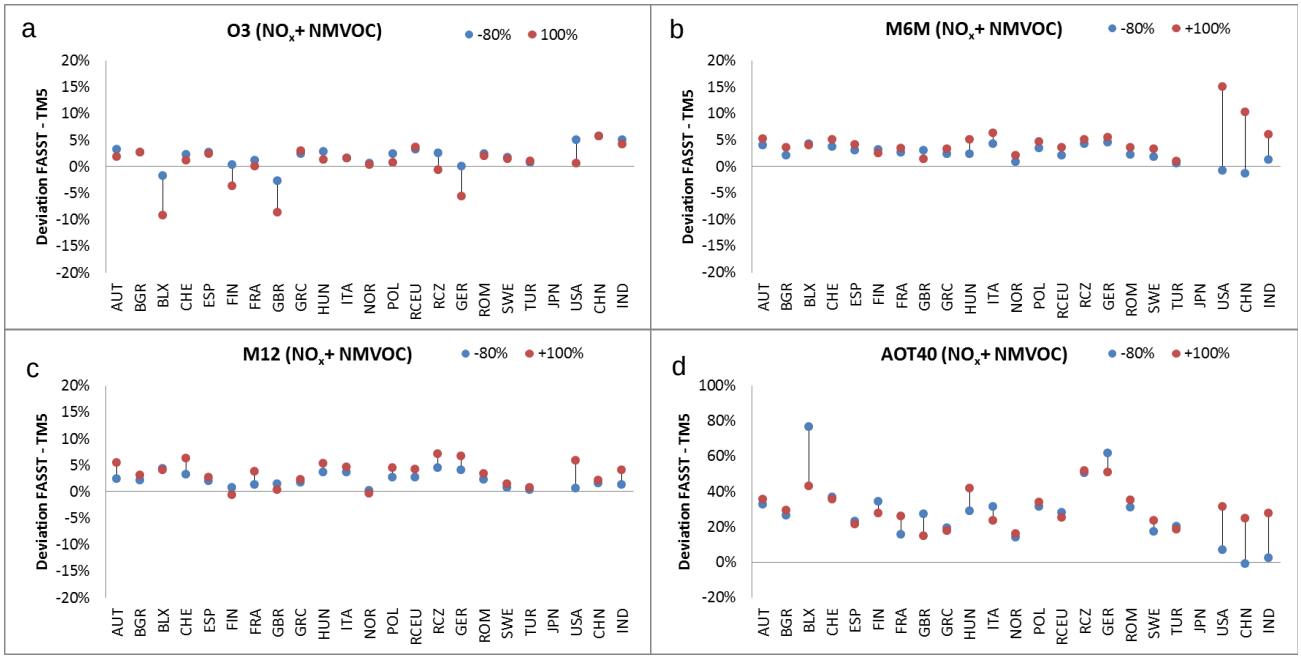

Figure S7.6 Same as Fig. S7.4, now for combined NO_x+NMVOC perturbations

S8 Supplemental information to section 3.2 - TM5-FASST_v0 versus TM5 for future emission scenarios

S8.1 Major features of the Global Energy Assesment scenarios used in the validation study

The GEA scenarios (Riahi, Dentener et al. 2012), consistent with similar long-term climate outcomes as the RCPs, are implemented in the MESSAGE model (Messner and Strubegger 1995; Riahi, Gruebler et al. 2007) and include more detailed representation of short-term air quality legislations from the GAINS model (Amann et al., 2011). A number of air pollutants are included in the scenario (SO_2, NO_x, CO, VOCs, BC, OC, total primary $PM_{2.5}$) air pollutants and are available at 0.5^o x 0.5^o resolution based on inventory data described in Lamarque et al. (2010), and an exposure-driven algorithm for the downscaling of the regional air-pollutant emissions projections. The GEA scenarios have been used to estimate global health impacts of outdoor air pollution (Rao et al., 2012, 2013) as well as for regional impacts analysis (Colette et al., 2012, 2013). We evaluate following pair:

1. FLE-2030 (Fixed Legislation scenario): This is a scenario with no improvement in air quality legislations beyond 2005. It thus serves to indicate a scenario with failure in terms of implementation of future air quality and climate policies and is used as a worst-case scenario, defining an upper boundary for the range of plausible air pollutant emission scenarios until 2030. In the literature this kind of scenarios is also referred to as Frozen legislation, or no-further-controls (NFC).
2. MIT-2030 (MITigation scenario): This scenario, consistent with long-term climate outcomes of the RCP2.6, assumes stringent climate mitigation policies consistent with a target of 2^oC global warming by the end of the century (2100), combined with stringent air quality legislations (SLE). Thus the MIT-2030 scenario provides a best-case scenario, defining the lower boundary of pollutant emission strengths. We evaluate the outcome in the year 2030.

Table S8: Relative emission changes for the test scenarios MIT-2030 and FLE-2030 compared to the year 2000 base scenario used for the 20% perturbation simulations.

	BC	NH3	NOx	POM	SO_2	NMVOC	PM2.5
				MIT-2030			
ASIA	-47%	+19%	-30%	-49%	-61%	-35%	+26%
LAM	-83%	-61%	-83%	-68%	-86%	-75%	-65%
MAF	-57%	-60%	-58%	-31%	-79%	-43%	-31%
OECD90	-89%	-41%	-73%	-80%	-90%	-81%	-74%
REF	-91%	-64%	-83%	-71%	-91%	-83%	-70%
GLOBAL	-49%	+25%	-64%	-36%	-72%	-39%	-6%
				FLE-2030			
ASIA	+97%	+21%	+165%	+20%	+98%	+53%	+245%
LAM	-74%	-61%	-60%	-66%	-72%	-54%	-59%
MAF	+7%	-59%	-7%	+20%	-17%	+44%	+18%
OECD90	-72%	-40%	-12%	-74%	-32%	-67%	-56%
REF	-82%	-64%	-53%	-66%	-51%	-73%	-58%
GLOBAL	+45%	+27%	+11%	+7%	+29%	+33%	+94%

OECD90: All countries that belonged to the Organization of Economic Development (OECD) as of 1990

MAF: Developing Countries in Middle East & Africa

LA:, All developing countries in Latin America

REF: Countries undergoing economic reform - East European countries and the Newly Independent States of the former Soviet Union

ASIA: All developing countries in Asia

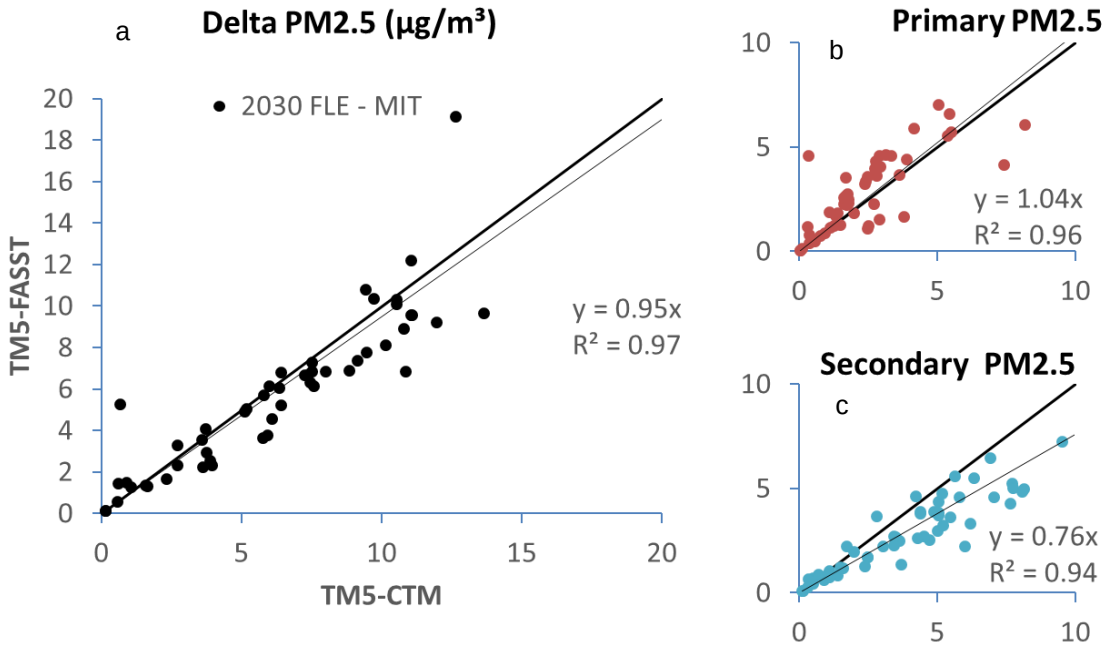

Figure S8.1 TM5-FASST vs. TM5_CTM change in anthropogenic $PM_{2.5}$ (a) between the GEA scenarios FLE-2030 and MIT-2030, and break-down for the primary (b) and secondary (c) fractions. Each point represent the population-weighted mean over a FASST source region.

5

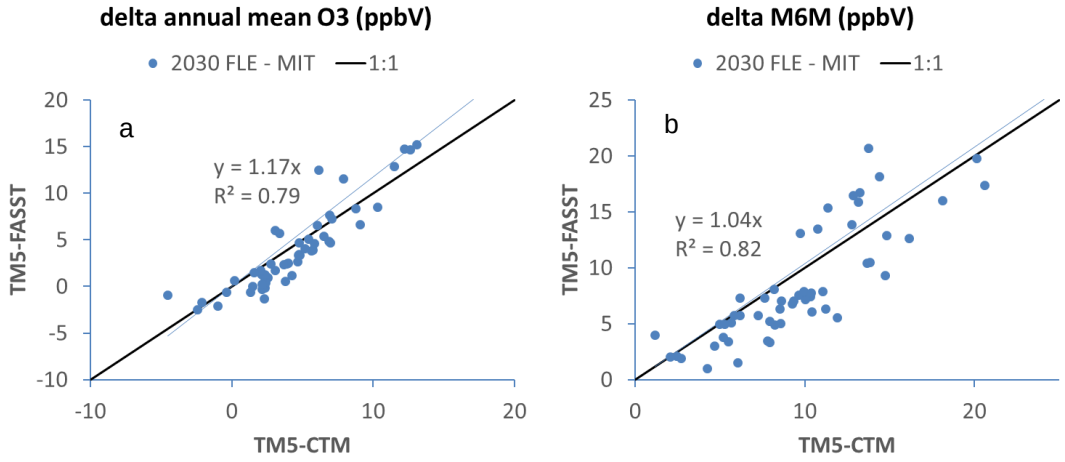

Figure S8.2 TM5-FASST versus TM5-CTM change in annual mean ozone (a) and exposure metric M6M (b) between the GEA scenarios FLE-2030 and MIT-2030. Each point represents the population-weighted mean over a FASST source region.

S9 Supplemental figures to section 3.3.4 - Health impacts: intercomparison with ACCMIP model ensemble

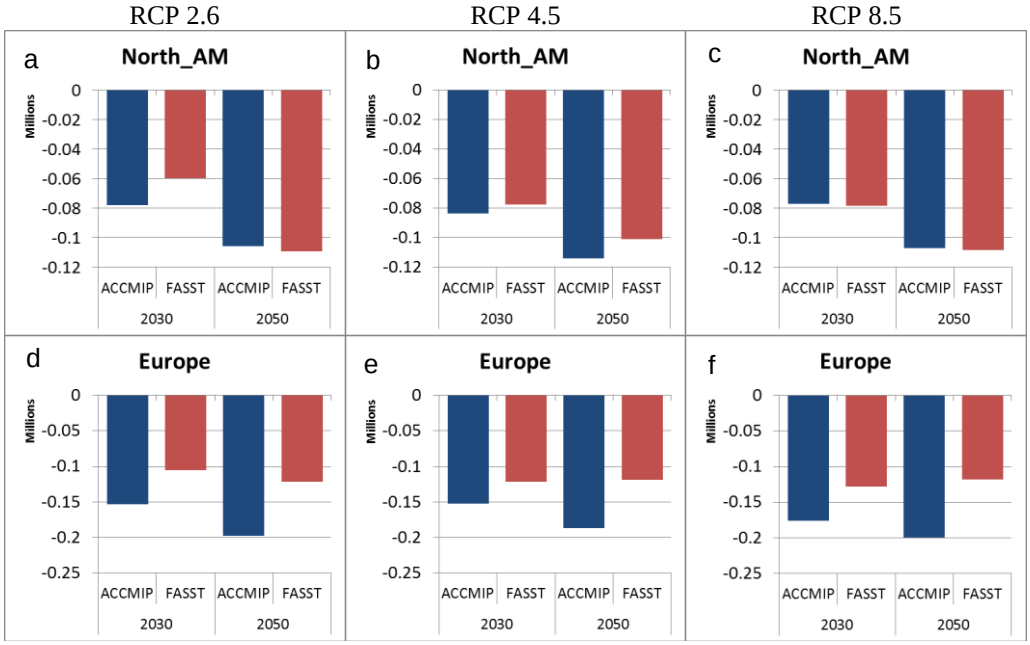

Figure S9: Mortality burden (million deaths) from $PM_{2.5}$ in 2030 and 2050 for RCP scenarios RCP 2.6 (a, d). RCP 4.5 (b, e) and RCP8.5 (c, f) relative to exposure to year 2000 concentrations, for North America (a to c) Europe and Europe (d to f). Blue bars: Mean of ACCMIP model ensemble results (Silva et al., 2016). Red bars: TM5-FASST.

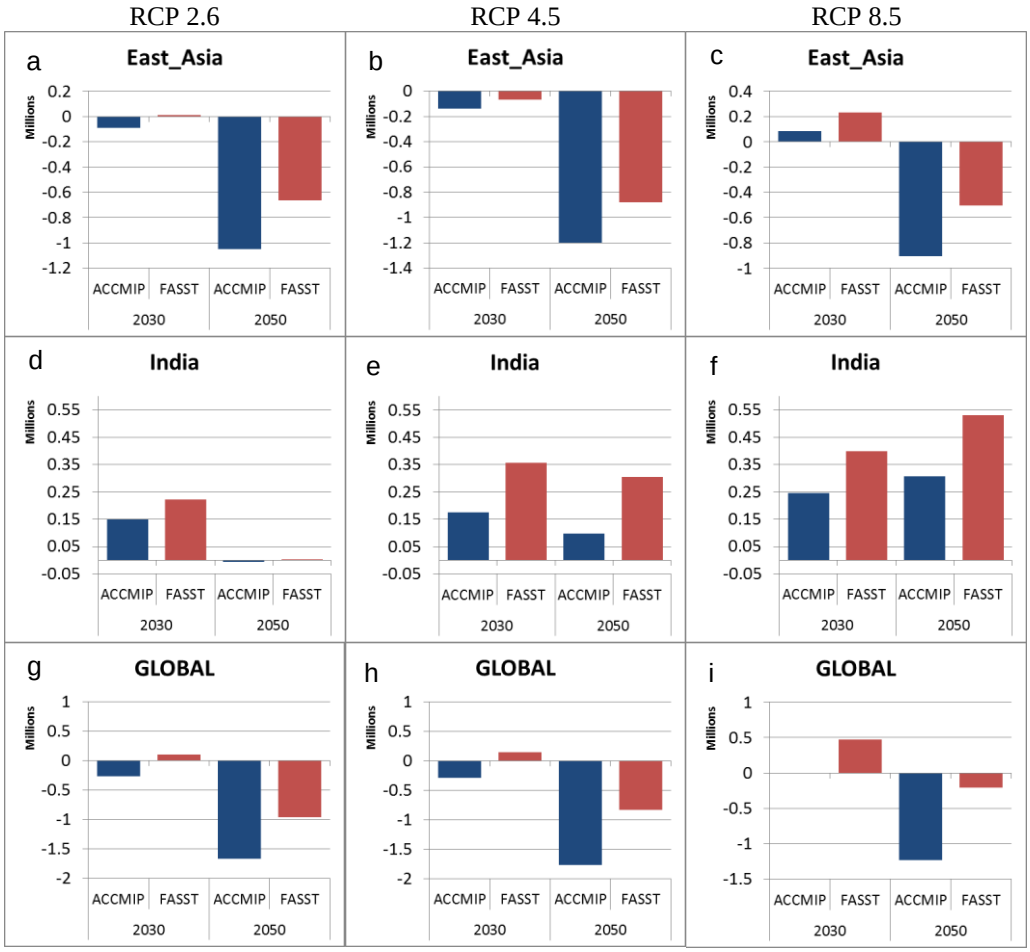

Figure S10: As in Fig. S9, now for regions East Asia (a to c), India (d to f) and the globe (g to i)

Supplemental Information - References

Amann, M., Bertok, I., Borken-Kleefeld, J., Cofala, J., Heyes, C., Höglund-Isaksson, L., Klimont, Z., Nguyen, B., Posch, M., Rafaj, P., Sandler, R., Schöpp, W., Wagner, F. and Winiwarter, W.: Cost-effective control of air quality and greenhouse gases in Europe: Modeling and policy applications, Environ. Model. Softw., 26(12), 1489–1501, doi:10.1016/j.envsoft.2011.07.012, 2011.

Bergamaschi, P., Krol, M., Dentener, F., Vermeulen, A., Meinhardt, F., Graul, R., Ramonet, M., Peters, W. and Dlugokencky, E. J.: Inverse modelling of national and European CH4 emissions using the atmospheric zoom model TM5, Atmospheric Chem. Phys., 5(9), 2431–2460, 2005.

Brauer, M., Amann, M., Burnett, R. T., Cohen, A., Dentener, F., Ezzati, M., Henderson, S. B., Krzyzanowski, M., Martin, R. V., Van Dingenen, R., Van Donkelaar, A. and Thurston, G. D.: Exposure assessment for estimation of the global burden of disease attributable to outdoor air pollution, Environ. Sci. Technol., 46(2), 652–660, doi:10.1021/es2025752, 2012.

Brauer, M., Freedman, G., Frostad, J., Van, D., Martin, R. V., Dentener, F., Dingenen, R. V., Estep, K., Amini, H., Apte, J. S., Balakrishnan, K., Barregard, L., Broday, D., Feigin, V., Ghosh, S., Hopke, P. K., Knibbs, L. D., Kokubo, Y., Liu, Y., Ma, S., Morawska, L., Sangrador, J. L. T., Shaddick, G., Anderson, H. R., Vos, T., Forouzanfar, M. H., Burnett, R. T. and Cohen, A.: Ambient Air Pollution Exposure Estimation for the Global Burden of Disease 2013, Environ. Sci. Technol., 50(1), 79–88, doi:10.1021/acs.est.5b03709, 2016.

Burnett, R. T., Pope, C. A., III, Ezzati, M., Olives, C., Lim, S. S., Mehta, S., Shin, H. H., Singh, G., Hubbell, B., Brauer, M., Anderson, H. R., Smith, K. R., Balmes, J. R., Bruce, N. G., Kan, H., Laden, F., Prüss-Ustün, A., Turner, M. C., Gapstur, S. M., Diver, W. R. and Cohen, A.: An Integrated Risk Function for Estimating the Global Burden of Disease Attributable to Ambient Fine Particulate Matter Exposure, Environ. Health Perspect., doi:10.1289/ehp.1307049, 2014.

CIESIN: Gridded Population of the World Version 3 (GPWv3), [online] Available from: http://sedac.ciesin.columbia.edu/gpw (Accessed 12 September 2012), 2005.

Cohen, A. J., Brauer, M., Burnett, R., Anderson, H. R., Frostad, J., Estep, K., Balakrishnan, K., Brunekreef, B., Dandona, L., Dandona, R., Feigin, V., Freedman, G., Hubbell, B., Jobling, A., Kan, H., Knibbs, L., Liu, Y., Martin, R., Morawska, L., Pope, C. A., III, Shin, H., Straif, K., Shaddick, G., Thomas, M., van Dingenen, R., van Donkelaar, A., Vos, T., Murray, C. J. L. and Forouzanfar, M. H.: Estimates and 25-year trends of the global burden of disease attributable to ambient air pollution: an analysis of data from the Global Burden of Diseases Study 2015, The Lancet, 389(10082), 1907–1918, doi:10.1016/S0140-6736(17)30505-6, 2017.

Colette, A., Granier, C., Hodnebrog, ø., Jakobs, H., Maurizi, A., Nyiri, A., Rao, S., Amann, M., Bessagnet, B., D'Angiola, A., Gauss, M., Heyes, C., Klimont, Z., Meleux, F., Memmesheimer, M., Mieville, A., Rouïl, L., Russo, F., Schucht, S., Simpson, D., Stordal, F., Tampieri, F. and Vrac, M.: Future air quality in Europe: A multi-model assessment of projected exposure to ozone, Atmospheric Chem. Phys., 12(21), 10613–10630, doi:10.5194/acp-12-10613-2012, 2012.

Colette, A., Bessagnet, B., Vautard, R., Szopa, S., Rao, S., Schucht, S., Klimont, Z., Menut, L., Clain, G., Meleux, F., Curci, G. and Rouïl, L.: European atmosphere in 2050, a regional air quality and climate perspective under CMIP5 scenarios, Atmospheric Chem. Phys., 13(15), 7451–7471, doi:10.5194/acp-13-7451-2013, 2013.

Crippa, M., Janssens-Maenhout, G., Dentener, F., Guizzardi, D., Sindelarova, K., Muntean, M., Van Dingenen, R. and Granier, C.: Forty years of improvements in European air quality: Regional policy-industry interactions with global impacts, Atmospheric Chem. Phys., 16(6), 3825–3841, doi:10.5194/acp-16-3825-2016, 2016.

Dana, M. T. and Hales, J. M.: Statistical aspects of the washout of polydisperse aerosols, Atmospheric Environ. 1967, 10(1), 45–50, doi:10.1016/0004-6981(76)90258-4, 1976.

De Meij, A., Krol, M., Dentener, F., Vignati, E., Cuvelier, C. and Thunis, P.: The sensitivity of aerosol in Europe to two different emission inventories and temporal distribution of emissions, Atmospheric Chem. Phys., 6(12), 4287–4309, 2006.

Dentener, F., Drevet, J., Lamarque, J. F., Bey, I., Eickhout, B., Fiore, A. M., Hauglustaine, D., Horowitz, L. W., Krol, M., Kulshrestha, U. C., Lawrence, M., Galy-Lacaux, C., Rast, S., Shindell, D., Stevenson, D., Van Noije, T., Atherton, C., Bell, N., Bergman, D., Butler, T., Cofala, J., Collins, B., Doherty, R., Ellingsen, K., Galloway, J., Gauss, M., Montanaro, V., Müller, J. F., Pitari, G., Rodriguez, J., Sanderson, M., Solmon, F., Strahan, S., Schultz, M., Sudo, K., Szopa, S. and Wild, O.: Nitrogen and sulfur deposition on regional and global scales: A multimodel evaluation, Glob. Biogeochem. Cycles, 20(4), GB4003, doi:10.1029/2005GB002672, 2006.

van Donkelaar, A., Martin, R. V., Brauer, M., Hsu, N. C., Kahn, R. A., Levy, R. C., Lyapustin, A., Sayer, A. M. and Winker, D. M.: Global Estimates of Fine Particulate Matter using a Combined Geophysical-Statistical Method with Information from Satellites, Models, and Monitors, Environ. Sci. Technol., 50(7), 3762–3772, doi:10.1021/acs.est.5b05833, 2016.

Fenn, R. W., Clough, S. A., Gallery, W. O., Good, R. E., Kneizys, F. X., Mill, J. D., Rothman, L. S., Shettle, E. P. and Volz, F. E.: Optical and infrared properties of the atmosphere, in Handbook of Geophysics and the Space Environment, vol. 18, pp. 1–27, Air Force Geophys. Lab., Hanscom Air Force Base, Bedford, Mass., 1985.

Ganzeveld, L. and Lelieveld, J.: Dry deposition parameterization in a chemistry general circulation model and its influence on the distribution of reactive trace gases, J. Geophys. Res., 100(D10), 20,999-21,012, 1995.

GEA: Global Energy Assessment - Toward a Sustainable Future, Cambridge University Press, Cambridge, UK and New York, NY, USA and the International Institute for Applied Systems Analysis, Laxenburg, Austria. [online] Available from: www.globalenergyassessment.org, 2012.

Gery, M. W., Whitten, G. Z., Killus, J. P. and Dodge, M. C.: A photochemical kinetics mechanism for urban and regional scale computer modeling, J. Geophys. Res., 94(D10), 12,925-12,956, 1989a.

Gery, M. W., Edmond, R. D. and Whitten, G. Z.: Potential effects of stratospheric ozone depletion and global temperature rise on urban photochemistry, Stud. Environ. Sci., 35(C), 365–375, doi:10.1016/S0166-1116(08)70604-6, 1989b.

Guelle, W., Balkanski, Y. J., Dibb, J. E., Schulz, M. and Dulac, F.: Wet deposition in a global size-dependent aerosol transport model 2. Influence of the scavenging scheme on 210Pb vertical profiles, surface concentrations, and deposition, J. Geophys. Res. Atmospheres, 103(D22), 28875–28891, 1998.

Hertel, O., Berkowicz, R., Christensen, J. and Hov, Ø.: Test of two numerical schemes for use in atmospheric transport-chemistry models, Atmospheric Environ. Part Gen. Top., 27(16), 2591–2611, doi:10.1016/0960-1686(93)90032-T, 1993.

Houweling, S., Dentener, F. and Lelieveld, J.: The impact of nonmethane hydrocarbon compounds on tropospheric photochemistry, J. Geophys. Res. Atmospheres, 103(3339), 10673–10696, 1998.

Huijnen, V., Williams, J., van Weele, M., van Noije, T., Krol, M., Dentener, F., Segers, A., Houweling, S., Peters, W., de Laat, J., Boersma, F., Bergamaschi, P., van Velthoven, P., Le Sager, P., Eskes, H., Alkemade, F., Scheele, R.,

Nédélec, P. and Pätz, H.-W.: The global chemistry transport model TM5: description and evaluation of the tropospheric chemistry version 3.0, Geosci. Model Dev., 3(2), 445–473, doi:10.5194/gmd-3-445-2010, 2010.

Jeuken, A., Veefkind, J. P., Dentener, F., Metzger, S. and Robles, G.: Simulation of the aerosol optical depth over Europe for August 1997 and a comparison with observations, J. Geophys. Res. Atmospheres, 106(D22), 28295–28311, 2001.

Kitous, A., Keramidas, K., Vandyck, T., Saveyn, B., Van Dingenen, R., Spadaro, J. and Holland, M.: Global Energy and Climate Outlook 2017: How climate policies improve air quality, Joint Research Centre (Seville site)., 2017.

Krol, M., Houweling, S., Bregman, B., van den Broek, M., Segers, A., van Velthoven, P., Peters, W., Dentener, F. and Bergamaschi, P.: The two-way nested global chemistry-transport zoom model TM5: algorithm and applications, Atmos Chem Phys, 5(2), 417–432, doi:10.5194/acp-5-417-2005, 2005.

Kuylenstierna, J. C. I., Zucca, M. C., Amann, M., Cardenas, B., Chambers, B., Klimont, Z., Hicks, K., Mills, R., Molina, L., Murray, F., Pearson, P., Sethi, S., Shindell, D., Sokona, Y., Terry, S., Vallack, H., Van Dingenen, R., Williams, M., Wilson, C. and Zusman, E.: Near-term climate protection and clean air benefits: Actions for controlling short-lived climate forcers, Report, United Nations Environment Programme, Nairobi, Kenya. [online] Available from: http://researchrepository.murdoch.edu.au/id/eprint/15325/ (Accessed 10 January 2017), 2011.

Lamarque, J.-F., Bond, T. C., Eyring, V., Granier, C., Heil, A., Klimont, Z., Lee, D., Liousse, C., Mieville, A., Owen, B., Schultz, M. G., Shindell, D., Smith, S. J., Stehfest, E., Van, A., Cooper, O. R., Kainuma, M., Mahowald, N., McConnell, J. R., Naik, V., Riahi, K. and Van, V.: Historical (1850-2000) gridded anthropogenic and biomass burning emissions of reactive gases and aerosols: Methodology and application, Atmospheric Chem. Phys., 10(15), 7017–7039, doi:10.5194/acp-10-7017-2010, 2010.

Li, J., Wong, J. G. D., Dobbie, J. S. and Chýlek, P.: Parameterization of the optical properties of sulfate aerosols, J. Atmospheric Sci., 58(2), 193–209, 2001.

Lim, S. S., Vos, T., Flaxman, A. D., Danaei, G., Shibuya, K., Adair-Rohani, H., Amann, M., Anderson, H. R., Andrews, K. G., Aryee, M., Atkinson, C., Bacchus, L. J., Bahalim, A. N., Balakrishnan, K., Balmes, J., Barker-Collo, S., Baxter, A., Bell, M. L., Blore, J. D., Blyth, F., Bonner, C., Borges, G., Bourne, R., Boussinesq, M., Brauer, M., Brooks, P., Bruce, N. G., Brunekreef, B., Bryan-Hancock, C., Bucello, C., Buchbinder, R., Bull, F., Burnett, R. T., Byers, T. E., Calabria, B., Carapetis, J., Carnahan, E., Chafe, Z., Charlson, F., Chen, H., Chen, J. S., Cheng, A. T.-A., Child, J. C., Cohen, A., Colson, K. E., Cowie, B. C., Darby, S., Darling, S., Davis, A., Degenhardt, L., Dentener, F., Des Jarlais, D. C., Devries, K., Dherani, M., Ding, E. L., Dorsey, E. R., Driscoll, T., Edmond, K., Ali, S. E., Engell, R. E., Erwin, P. J., Fahimi, S., Falder, G., Farzadfar, F., Ferrari, A., Finucane, M. M., Flaxman, S., Fowkes, F. G. R., Freedman, G., Freeman, M. K., Gakidou, E., Ghosh, S., Giovannucci, E., Gmel, G., Graham, K., Grainger, R., Grant, B., Gunnell, D., Gutierrez, H. R., Hall, W., Hoek, H. W., Hogan, A., Hosgood III, H. D., Hoy, D., Hu, H., Hubbell, B. J., Hutchings, S. J., Ibeanusi, S. E., Jacklyn, G. L., Jasrasaria, R., Jonas, J. B., Kan, H., Kanis, J. A., Kassebaum, N., Kawakami, N., Khang, Y.-H., Khatibzadeh, S., Khoo, J.-P., Kok, C., et al.: A comparative risk assessment of burden of disease and injury attributable to 67 risk factors and risk factor clusters in 21 regions, 1990-2010: A systematic analysis for the Global Burden of Disease Study 2010, The Lancet, 380(9859), 2224–2260, doi:10.1016/S0140-6736(12)61766-8, 2012.

Lund Myhre, C. E. and Nielsen, C. J.: Optical properties in the UV and visible spectral region of organic acids relevant to tropospheric aerosols, Atmos Chem Phys, 4(7), 1759–1769, doi:10.5194/acp-4-1759-2004, 2004.

Nemesure, S., Wagener, R. and Schwartz, S. E.: Direct shortwave forcing of climate by the anthropogenic sulfate aerosol: Sensitivity to particle size, composition, and relative humidity, J. Geophys. Res. Atmospheres, 100(D12), 26105–26116, doi:10.1029/95JD02897, 1995.

van Noije, T. P. C., Eskes, H. J., Dentener, F. J., Stevenson, D. S., Ellingsen, K., Schultz, M. G., Wild, O., Amann, M., Atherton, C. S., Bergmann, D. J., Bey, I., Boersma, K. F., Butler, T., Cofala, J., Drevet, J., Fiore, A. M., Gauss, M., Hauglustaine, D. A., Horowitz, L. W., Isaksen, I. S. A., Krol, M. C., Lamarque, J.-F., Lawrence, M. G., Martin, R. V., Montanaro, V., Müller, J.-F., Pitari, G., Prather, M. J., Pyle, J. A., Richter, A., Rodriguez, J. M., Savage, N. H., Strahan, S. E., Sudo, K., Szopa, S. and van Roozendael, M.: Multi-model ensemble simulations of tropospheric NO2 compared with GOME retrievals for the year 2000, Atmos Chem Phys, 6(10), 2943–2979, doi:10.5194/acp-6-2943-2006, 2006.

OECD: The Economic Consequences of Outdoor Air Pollution, OECD Publishing. [online] Available from: http://www.oecd-ilibrary.org/environment/the-economic-consequences-of-outdoor-air-pollution_9789264257474-en (Accessed 10 January 2017), 2016.

Penner, J. E., Chuang, C. C. and Grant, K.: Climate forcing by carbonaceous and sulfate aerosols, Clim. Dyn., 14(12), 839–851, doi:10.1007/s003820050259, 1998.

Peters, W.: Toward regional-scale modeling using the two-way nested global model TM5: Characterization of transport using SF_6, J. Geophys. Res., 109(D19), doi:10.1029/2004JD005020, 2004.

Petersen, A. C., Spee, E. J., Van, D. and Hundsdorfer, W.: An evaluation and intercomparison of four new advection schemes for use in global chemistry models, J. Geophys. Res. Atmospheres, 103(D15), 19253–19269, 1998.

Rao, S., Chirkov, V., Dentener, F., Van Dingenen, R., Pachauri, S., Purohit, P., Amann, M., Heyes, C., Kinney, P., Kolp, P., Klimont, Z., Riahi, K. and Schoepp, W.: Environmental Modeling and Methods for Estimation of the Global Health Impacts of Air Pollution, Environ. Model. Assess., 17(6), 613–622, doi:10.1007/s10666-012-9317-3, 2012.

Rao, S., Pachauri, S., Dentener, F., Kinney, P., Klimont, Z., Riahi, K. and Schoepp, W.: Better air for better health: Forging synergies in policies for energy access, climate change and air pollution, Glob. Environ. Change, 23(5), 1122–1130, doi:10.1016/j.gloenvcha.2013.05.003, 2013.

Rao, S., Klimont, Z., Leitao, J., Riahi, K., Van Dingenen, R., Reis, L. A., Katherine Calvin, Dentener, F., Drouet, L., Fujimori, S., Harmsen, M., Luderer, G., Chris Heyes, Strefler, J., Tavoni, M. and Vuuren, D. P. van: A multi-model assessment of the co-benefits of climate mitigation for global air quality, Environ. Res. Lett., 11(12), 124013, doi:10.1088/1748-9326/11/12/124013, 2016.

Rao, S., Klimont, Z., Smith, S. J., Van Dingenen, R., Dentener, F., Bouwman, L., Riahi, K., Amann, M., Bodirsky, B. L., van Vuuren, D. P., Aleluia Reis, L., Calvin, K., Drouet, L., Fricko, O., Fujimori, S., Gernaat, D., Havlik, P., Harmsen, M., Hasegawa, T., Heyes, C., Hilaire, J., Luderer, G., Masui, T., Stehfest, E., Strefler, J., van der Sluis, S. and Tavoni, M.: Future air pollution in the Shared Socio-economic Pathways, Glob. Environ. Change, 42, 346–358, doi:10.1016/j.gloenvcha.2016.05.012, 2017.

Riahi, K., Dentener, F., Gielen, D., Grubler, A., Jewell, J., Klimont, Z., Krey, V., McCollum, D., Pachauri, S., Rao, S., van Ruijven, B., van Vuuren, D. P. and Wilson, C.: The Global Energy Assessment - Chapter 17 - Energy Pathways for Sustainable Development, in Global Energy Assessment - Toward a Sustainable Future, pp. 1203–1306, Cambridge University Press, Cambridge, UK and New York, NY, USA and the International Institute for Applied Systems Analysis, Laxenburg, Austria. [online] Available from: www.globalenergyassessment.org, 2012.

Russell, G. L. and Lerner, J. A.: A New Finite-Differencing Scheme for the Tracer Transport Equation, J. Appl. Meteorol., 20(12), 1483–1498, doi:10.1175/1520-0450(1981)020<1483:ANFDSF>2.0.CO;2, 1981.

Shindell, D. T., Chin, M., Dentener, F., Doherty, R. M., Faluvegi, G., Fiore, A. M., Hess, P., Koch, D. M., MacKenzie, I. A., Sanderson, M. G., Schultz, M. G., Schulz, M., Stevenson, D. S., Teich, H., Textor, C., Wild, O., Bergmann, D. J., Bey, I., Bian, H., Cuvelier, C., Duncan, B. N., Folberth, G., Horowitz, L. W., Jonson, J., Kaminski, J. W., Marmer, E.,

Park, R., Pringle, K. J., Schroeder, S., Szopa, S., Takemura, T., Zeng, G., Keating, T. J. and Zuber, A.: A multi-model assessment of pollution transport to the Arctic, Atmos Chem Phys, 8(17), 5353–5372, doi:10.5194/acp-8-5353-2008, 2008.

Silva, R. A., West, J. J., Lamarque, J. F., Shindell, D. T., Collins, W. J., Dalsoren, S., Faluvegi, G., Folberth, G., Horowitz, L. W., Nagashima, T., Naik, V., Rumbold, S. T., Sudo, K., Takemura, T., Bergmann, D., Cameron-Smith, P., Cionni, I., Doherty, R. M., Eyring, V., Josse, B., MacKenzie, I. A., Plummer, D., Righi, M., Stevenson, D. S., Strode, S., Szopa, S. and Zengast, G.: The effect of future ambient air pollution on human premature mortality to 2100 using output from the ACCMIP model ensemble, Atmospheric Chem. Phys., 16(15), 9847–9862, doi:10.5194/acp-16-9847-2016, 2016.

Sloane, C. S.: Optical properties of aerosols—comparison of measurements with model calculations, Atmospheric Environ. 1967, 17(2), 409–416, doi:10.1016/0004-6981(83)90059-8, 1983.

Textor, C., Schulz, M., Guibert, S., Kinne, S., Balkanski, Y., Bauer, S., Berntsen, T., Berglen, T., Boucher, O., Chin, M., Dentener, F., Diehl, T., Easter, R., Feichter, H., Fillmore, D., Ghan, S., Ginoux, P., Gong, S., Grini, A., Hendricks, J., Horowitz, L., Huang, P., Isaksen, I., Iversen, I., Kloster, S., Koch, D., Kirkevåg, A., Kristjansson, J. E., Krol, M., Lauer, A., Lamarque, J. F., Liu, X., Montanaro, V., Myhre, G., Penner, J., Pitari, G., Reddy, S., Seland, Ø., Stier, P., Takemura, T. and Tie, X.: Analysis and quantification of the diversities of aerosol life cycles within AeroCom, Atmos Chem Phys, 6(7), 1777–1813, doi:10.5194/acp-6-1777-2006, 2006.

The World Bank, The International Cryosphere Climate Initiative: On Thin Ice, Washington DC. [online] Available from: http://iccinet.org/thinicepubfinal, 2013.

Toon, O. B., Pollack, J. B. and Khare, B. N.: The optical constants of several atmospheric aerosol species: Ammonium sulfate, aluminum oxide, and sodium chloride, J. Geophys. Res., 81(33), 5733–5748, doi:10.1029/JC081i033p05733, 1976.

UN DESA: World Population Prospects: The 2008 Revision Database., Working Paper, United Nations Department of Economic and Social Affairs (UN DESA), New York., 2009.

UNEP and CCAC: Integrated Assessment of Short-Lived Climate Pollutants for Latin America and the Caribbean: improving air quality while mitigating climate change. Summary for decision makers., United Nations Environmenal Programme, Nairobi, Kenya. [online] Available from: http://www.ccacoalition.org/sites/default/files/resources/UNEP_Assessment%20A%20SINGLE.pdf (Accessed 14 December 2017), 2016.

Van Dingenen, R., Dentener, F. J., Raes, F., Krol, M. C., Emberson, L. and Cofala, J.: The global impact of ozone on agricultural crop yields under current and future air quality legislation, Atmos. Environ., 43(3), 604–618, doi:10.1016/j.atmosenv.2008.10.033, 2009.

Vignati, E., Karl, M., Krol, M., Wilson, J., Stier, P. and Cavalli, F.: Sources of uncertainties in modelling black carbon at the global scale, Atmospheric Chem. Phys., 10(6), 2595–2611, 2010.

Wehrli, C.: Solar Spectral Irradiance: Wehrli 1985 AM0 Spectrum, Wehrli 1985 AM0 Spectr. [online] Available from: http://rredc.nrel.gov/solar/spectra/am0/wehrli1985.new.html (Accessed 18 December 2017), 1985.

van der Werf, G. R., Randerson, J. T., Collatz, G. J., Louis Giglio, Kasibhatla, P. S., Arellano, A. F., Olsen, S. C. and Kasischke, E. S.: Continental-Scale Partitioning of Fire Emissions During the 1997 to 2001 El Niño/La Niña Period, Science, 303(5654), 73–76, doi:10.1126/science.1090753, 2004.

van Zelm, R., Preiss, P., van Goethem, T., Van Dingenen, R. and Huijbregts, M.: Regionalized life cycle impact assessment of air pollution on the global scale: Damage to human health and vegetation, Atmos. Environ., 134, 129–137, doi:10.1016/j.atmosenv.2016.03.044, 2016.

5